SYMBOL TIMING RECOVERY FOR CPM SIGNALS BASED ON MATCHED FILTERING

A THESIS SUBMITTED TO
THE GRADUATE SCHOOL OF NATURAL AND APPLIED SCIENCES
OF
MIDDLE EAST TECHNICAL UNIVERSITY

BY

ÇİLER BAŞERDEM

IN PARTIAL FULFILLMENT OF THE REQUIREMENTS
FOR
THE DEGREE OF MASTER OF SCIENCE
IN
THE DEPARTMENT OF ELECTRICAL AND ELECTRONICS ENGINEERING

DECEMBER 2006

Approval of the Graduate School of Natural and Applied Sciences

Prof. Dr. Canan Özgen
Director

I certify that this thesis satisfies all the requirements as a thesis for the degree of Master of Science.

Prof. Dr. İsmet Erkmen
Head of Department

This is to certify that we have read this thesis and that in our opinion it is fully adequate, in scope and quality, as a thesis for the degree of Master of Science.

Prof. Dr. Yalçın Tanık
Supervisor

Examining Committee Members

Prof. Dr. Mete Severcan	(METU, EE)	
Prof. Dr. Yalçın Tanık	(METU, EE)	
Prof. Dr. Kerim Demirbaş	(METU, EE)	
Assist. Prof. Dr. Ali Özgür Yılmaz	(METU, EE)	
Çağdaş Enis Doyuran (M.S.)	(ASELSAN)	

I hereby declare that all information in this document has been obtained and presented in accordance with academic rules and ethical conduct. I also declare that, as required by these rules and conduct, I have fully cited and referenced all material and results that are not original to this work.

Name, Last name : Çiler Başerdem

Signature :

ABSTRACT

SYMBOL TIMING RECOVERY FOR CPM SIGNALS
BASED ON MATCHED FILTERING

Başerdem, Çiler
M.S., Department of Electrical and Electronics Engineering
Supervisor : Prof. Dr. Yalçın Tanık

December 2006, 96 pages

In this thesis, symbol timing recovery based on matched filtering in Gaussian Minimum Shift Keying (GMSK) with bandwidth-bit period product (BT) of 0.3 is investigated. GMSK is the standard modulation type for GSM. Although GMSK modulation is non-linear, it is approximated to Offset Quadrature Amplitude Modulation (OQAM), which is a linear modulation, so that Maximum Likelihood Sequence Estimation (MLSE) method is possible in the receiver part. In this study Typical Urban (TU) channel model developed in COST 207 is used. Two methods are developed on the construction of the matched filter. In order to obtain timing recovery for GMSK signals, these methods are investigated. The fractional time delays are acquired by using interpolation and an iterative maximum search process. The performance of the proposed symbol timing recovery (STR) scheme is assessed by using computer simulations. It is observed that the STR tracks the variations of the frequency selective multipath fading channels almost the same as the Mazo criterion.

Keywords: Symbol timing recovery, Gaussian Minimum Shift Keying (GMSK), matched filtering, multipath fading channel, Mazo criterion.

ÖZ

CPM SİNYALLERİ İÇİN UYUMLU SÜZGEÇLEMEYE DAYALI SEMBOL ZAMAN BİLGİSİNİN KAZANIMI

Başerdem, Çiler
Yüksek Lisans, Elektrik ve Elektronik Mühendisliği Bölümü
Tez Yöneticisi : Prof. Dr. Yalçın Tanık

Aralık 2006, 96 sayfa

Bu tezde, bant genişliği ile bit aralığı çarpımı 0.3 olan Gaussian en küçük kaydırmalı kiplenim (GMSK) sinyalleri için uyumlu süzgeçlemeye dayalı sembol zaman bilgisinin kazanımı incelenmiştir. GMSK, GSM sistemi için standart modülasyon tipidir. GMSK modülasyonu, doğrusal olmamasına rağmen, en büyük olasılıklı dizi kestirimi (MLSE) yönteminin alıcı kısmında kullanılabilmesi için doğrusal bir modülasyon tipi olan OQAM' ye benzetilmiştir. Bu çalışmada COST 207 'de geliştirilen şehiriçi tipik kanal modeli kullanılmıştır. Uyumlu süzgeç yapısı için iki yöntem geliştirilmiştir. GMSK sinyalleri için zaman bilgisinin kazanımını elde etmek amacıyla bu iki yöntem incelenmiştir. Ufak zaman gecikmeleri, aradeğerleme ve döngülü en yüksek arama yöntemleri kullanılarak elde edilmiştir. Önerilen sembol zaman kazanım (STR) yapısının başarımı bilgisayar benzetimleri kullanılarak değerlendirilmiştir. STR'nin frekans seçici çokyönlü sönümlemeli kanal değişimlerini Mazo ölçütüne çok benzer takip ettiği gözlenmiştir.

Anahtar kelimeler: Sembol zaman kazanımı, Gaussian en küçük kaydırmalı kiplenim , uyumlu süzgeç, çokyönlü sönümlemeli kanal, Mazo ölçütü.

To my family

ACKNOWLEDGMENTS

I would like to express my appreciation to my supervisor Prof. Dr. Yalçın Tanık for his supervision, support and helpful comments on this thesis.

I am also grateful to ASELSAN Inc. for letting and supporting of my thesis.

Additionally I would like to thank to Çağdaş Enis Doyuran for his motivative comments and great contributions about writing this thesis.

I also wish to express my deep gratitude to my parents and my dear brother, for their support during my life.

Finally, special thanks are due to my colleague Hazım Tokuçcu for his great support, encouragement and patience throughout my thesis study.

TABLE OF CONTENTS

LIST OF TABLES

TABLES

LIST OF FIGURES

FIGURES

LIST OF ABBREVIATIONS

BT	Bandwidth-Bit Period Product
BU	Bad Urban
CIR	Channel Impulse Response
CPM	Continuous Phase Modulation
CRB	Cramer Rao Bound
DA	Data-aided
DD	Decision-Directed
DECT	Digital enhanced cordless telephone
GMSK	Gaussian Minimum Shift Keying
GSM	Global Systems Mobile Communications
HT	Hilly Terrain
ISI	Intersymbol Interference
LLF	Log Likelihood Function
MCRB	Modified Cramer Rao Bound
ML	Maximum Likelihood
MLSE	Maximum Likelihood Sequence Estimation
MMSE	Minimum Mean Square Estimation
msISI	Minimum Squared Intersymbol Interference
MSK	Minimum Shift Keying
NCO	Number Controlled Oscillator

NDA	Non-Data Aided
NDD	Non-Decision Directed
OQAM	Offset Quadrature Amplitude Modulation
RA	Rural Area
STR	Symbol Timing Recovery
TED	Timing Error Detector
TSC	Training Sequence Code
TU	Typical Urban

CHAPTER 1

INTRODUCTION

1.1 SCOPE AND OBJECTIVE

Symbol synchronization or symbol timing recovery is a crucial part of the receiver in synchronous communication systems. The timing information depends on the overall system impulse response thus, on the characteristics of the communication channel. Most of the practical synchronizers have been based on transmission systems with no intersymbol interference (ISI) or with a time spread less than a symbol period, which is not realistic at all. On the other hand, multipath fading channel with a large delay spread causes ISI, so determination of the sampling instant is a much more difficult problem. Therefore transmission over frequency-selective fading channels necessitates specifically designed synchronizer structures and algorithms. Feedforward approaches based on maximum likelihood estimation are good candidates because of their rapid acquisition of symbol timing with the absence of hang-up problems, which are very common for feedback configurations.

Symbol timing recovery of continuous phase modulation (CPM) signals has taken considerable attention due to the attractive characteristics of the signal. CPM is a constant envelope, nonlinear modulation method which conserves and reduces energy and bandwidth at the same time. Minimum shift keying (MSK) and Gaussian minimum shift keying (GMSK) are the special forms of CPM. The modulation scheme chosen by GSM is GMSK with a bandwidth symbol period product of BT=0.3. Also GMSK with BT=0.5 is the modulation of the DECT system.

A timing recovery algorithm for MSK signals, which is able to extract the fractional delays even in the presence of severe channel variation, is presented in [1]. The proposed method in [1] (and also in [2]) eliminates the cycle slips very successfully. The recovery of the timing epoch is performed with matched filter method, together with an interpolator and an iterative maximum search process. [1] claims that the proposed recovery scheme is modulation independent and applicable to any modulation type as CPM signals.

The objective of this thesis study is to examine symbol timing recovery for GMSK which is one of the most popular modulation types of CPM signal used in GSM. In this study, in order to investigate the performance of the proposed recovery scheme (in [1] and [2]) in GMSK, two methods are developed on the construction of the matched filter. Timing estimation for the GMSK is obtained by using one of these methods and precise timing estimation is achieved by employing interpolation and iterative maximum search process. Timing recovery scheme consists of two modes. In acquisition mode, a data-aided approach is used for the adjustment of the initial timing. Training sequence known by the receiver is used. In tracking mode, tracking of the channel variation is performed with decision-directed timing recovery, error free tentative decisions from MLSE receiver are assumed. Mazo criterion is reviewed and used in order to assess the performance of the synchronizer.

1.2 OUTLINE OF THE STUDY

The thesis has the following outline:

In Chapter 2, the model of multipath fading channel, linear approximated GMSK signal and the MLSE receiver structure are presented.

Basic timing recovery methods and maximum likelihood estimation of the timing epoch are reviewed in Chapter 3.

In Chapter 4, important tools; modified Cramer-Rao bound and one of the possible criteria; Mazo criteria are presented in order to assess performance of the synchronizer. Then, the proposed timing recovery scheme, consisting of correlation method, interpolation and the iterative maximum search algorithm in [1], is reviewed. Finally, parameters which affect the performance of the timing recovery scheme are discussed.

The simulations and results are presented in Chapter 5. The simulated system is described in detail. Methods developed on construction of the matched filter are discussed which are special for GMSK application. Tracking ability of the proposed timing scheme for GMSK is presented through the simulation results.

In the last chapter, conclusions and possible future work are presented.

The general form of the CPM signals and especially MSK and GMSK signals are given in Appendix A.

In Appendix B, approximation of GMSK signal to linear QAM signal is presented in detail.

CHAPTER 2

BACKGROUND MATERIAL

2.1 INTRODUCTION

In radio channels the received signal is the sum of a number of signals arriving through different propagation paths. Each signal path is affected by a random amplitude attenuation and a phase shift that tend to change over time. Due to the multipath nature of the communication channel, interference occurs between adjacent symbols, which is known as intersymbol interference (ISI). The maximum likelihood sequence estimation (MLSE) technique has the best performance for demodulating operations over channels with ISI and additive white Gaussian noise.

In this chapter model of multipath fading channels and MLSE receiver for GMSK signals are presented.

2.2 CHANNEL MODEL

The mobile radio channel is based on the propagation of radio waves in a complex transmission environment. For mobile radio applications, the channel is time-varying because the motion between the transmitter and receiver results in propagation path changes.

2.2.1 Characterization of Multipath Fading Channel

From [1] the equivalent low-pass channel is expressed by time-variant response

$$h_c(\Delta t;t) = \sum_n \alpha_n(t)\delta(\Delta t - \Delta t_n), \tag{2.1}$$

where h_c (Δt;t) represents the response of the channel at time t due to an impulse applied at time Δt-t [3] The complex process, $\alpha_n(t)$ can be represented as

$$\alpha_n(t) = c_n(t)e^{-jw_c\Delta t_n}, \tag{2.2}$$

where Δt_n is the propagation delay and $c_n(t)$ is the attenuation factor for the n-th path. The low-pass equivalent of the fading channel model may be depicted as in Figure 2.1.

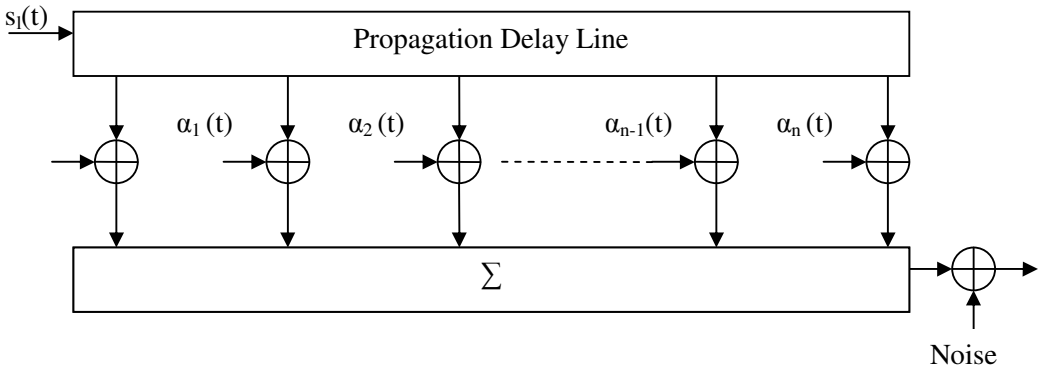

Figure 2.1 Multipath fading channel model.

2.2.2 Channel Statistical Characterization:

The scattering function S(*Δt;f)* is the most important statistical measure of the random multipath channel. It is a function of two variables; *Δt* (delay) and a frequency domain variable *f* is called the Doppler frequency. The scattering function provides a single measure of the average power output of the channel as a function of the delay *Δt* and the *f* Doppler frequency. In other words, the scattering function describes the manner in which the transmitted power is distributed in time and frequency, upon passing through the channel. From the scattering function we can obtain some of the most important relationships of a channel which impact the performance of a communication system operating over that channel.

The delay-power profile P (Δt), which is also referred to as the multipath intensity profile, is related to the scattering function via

$$P(\Delta t) = \int_{-\infty}^{\infty} S(\Delta t, f)df \ . \tag{2.3}$$

Another function that is useful in characterizing fading is the Doppler power spectrum, which is derived from the scattering function through

$$S(f) = \int_{-\infty}^{\infty} S(\Delta t, f)d\Delta t \ . \tag{2.4}$$

Different propagation models can be described by defining discrete number of taps, each determined by their time delay and average power.

2.2.2.1 Doppler Power Spectrum

Doppler spectrum *S(f)* determines the time variations of the channel. When *S(f)* is equal to the delta function , the channel becomes to be time-invariant.

For modeling of the channel, three types of Doppler spectra is defined in COST 207 final report; classical Doppler spectrum, Gauss 1 and Gauss 2 [4]. The most commonly used, and in a certain sense, the worst case Doppler spectrum is the classical Doppler spectrum which is also called *Jakes spectrum*. In this spectrum type, all the angle between vehicle speed and radio wave are assumed to be equally probable [5]. The classical Doppler spectrum

$$S(f) = \frac{A}{\left[1-(f/f_d)^2\right]^{1/2}} \qquad \text{for } f \in (-f_d, f_d), \tag{2.5}$$

where f_d is maximum Doppler shift, and

$$f_d = \frac{v}{c} \cdot f_c, \tag{2.6}$$

where v is the velocity of the mobile and f_c the carrier frequency. The classical Doppler spectrum is used throughout this study.

Classical Doppler spectrum for a mobile speed of 90 km/h and a carrier frequency of 1800 MHz is shown in Figure 2.2.

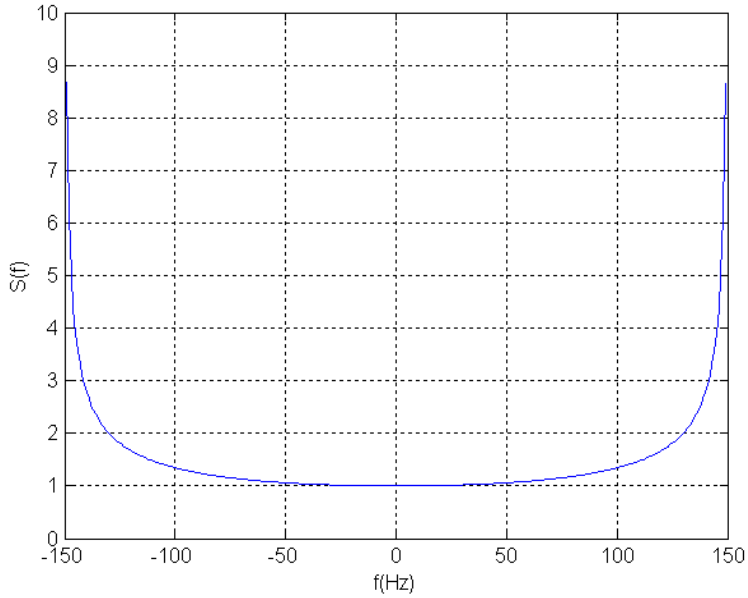

Figure 2.2 Classical doppler spectrum (f_d = 150 Hz).

2.2.2.2 Delay Power Profile

The average power for each tap is described by the delay power profile, P(Δt_n) .The delay power profiles are defined as

$$P(\Delta t_n) = P_0 \int_{-f_d}^{f_d} S(\Delta t_n, f)df \ , \tag{2.7}$$

where P(Δt_n) is the power transmitted by tap n and P_0 is the normalizing power. The continuous delay power profiles P(Δt) are defined in COST 207 as follows;

a) Typical case for rural (non-hilly) area (RA);

$$P(\Delta t) = \begin{cases} e^{-9.2\Delta t} & \text{for} \quad 0 < \Delta t < 7\mu\text{s} \\ 0 & \text{elsewhere} \end{cases} \tag{2.8}$$

b) Typical case for urban (non-hilly) area (TU);

$$P(\Delta t) = \begin{cases} e^{-\Delta t} & \text{for} \quad 0 < \Delta t < 7\mu\text{s} \\ 0 & \text{elsewhere} \end{cases} \tag{2.9}$$

Power delay profile for TU channel is shown in Figure 2.3

c) Typical bad case for hilly urban area (Bad Urban-BU);

$$P(\Delta t) = \begin{cases} e^{-\Delta t} & \text{for} \quad 0 < \Delta t < 5\mu\text{s} \\ 0.5e^{5-\Delta t} & \text{for} \quad 5 < \Delta t < 10\mu\text{s} \\ 0 & \text{elsewhere} \end{cases} \tag{2.10}$$

d) Typical case for hilly terrain (HT);

$$P(\Delta t) = \begin{cases} e^{-3.5\Delta t} & \text{for} \quad 0 < \Delta t < 2\mu\text{s} \\ 0.1e^{15-\Delta t} & \text{for} \quad 15 < \Delta t < 20\mu\text{s} \\ 0 & \text{elsewhere} \end{cases} \tag{2.11}$$

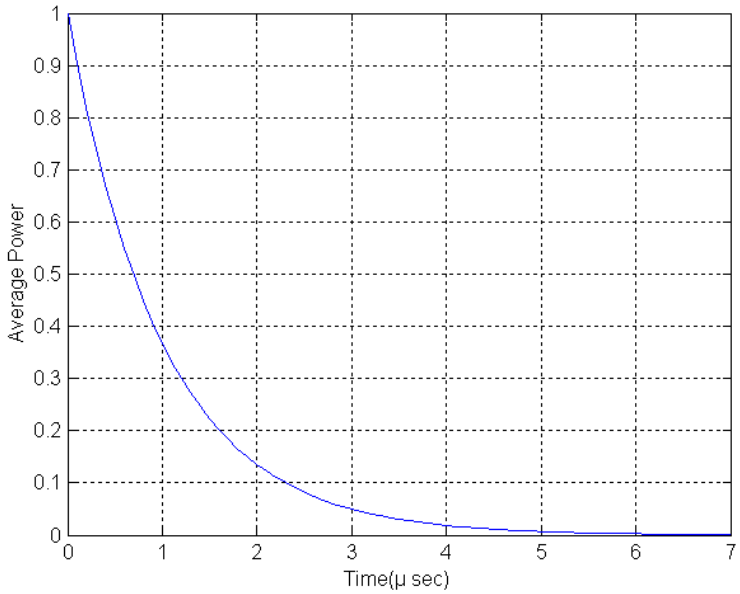

Figure 2.3 Power delay profile for Typical Urban (TU) channel.

2.2.3 Generation of Tap-Gain Processes:

In order to obtain the tap gain, it is sufficient to generate a signal whose frequency response is the scattering function. This can be accomplished by properly filtering white noise as shown in Figure 2.4. The flatness of the frequency spectrum of the filtering white noise results in simplification on the design of the shaping filter.

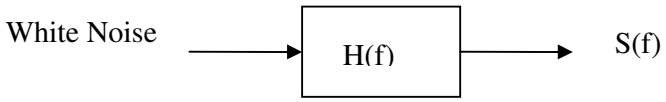

Figure 2.4 Filtering of white noise.

$$S(f) = \left|H(f)\right|^2 S_w(f). \tag{2.12}$$

$S_w(f)$ is the power spectral density of the white noise. Since the power spectral density of the white noise is a constant for all frequencies, the magnitude of the shaping filter response $H(f)$ becomes

$$\left|H(f)\right| = \sqrt{S(f)}. \tag{2.13}$$

$$H(f) = \frac{A^{1/2}}{\left[1-(f/f_d)^2\right]^{1/4}}. \tag{2.14}$$

$$h(t) = A^{1/2}\, 2.583\, f_d\, x^{-1/4}\, J_{1/4}(x), \tag{2.15}$$

where $J_{1/4}(.)$ is the fractional Bessel function and $x = 2\pi f_d |t|$. The shaping filter gain $A^{1/2}$ is chosen such that $h(t)$ has the normalized power of 1.

The individual tap gains $\alpha_n(t)$ then have to be properly scaled to account for different powers of the taps as shown in Figure 2.5. In order to calibrate tap gains, delay power profile $P(\Delta t)$ is used. From [5]

$$E[|\alpha_n(t)^2|] = \sigma_n^2 = \Delta t^2 \, P(n\Delta t), \tag{2.16}$$

where σ_n is the standard deviation for each n.

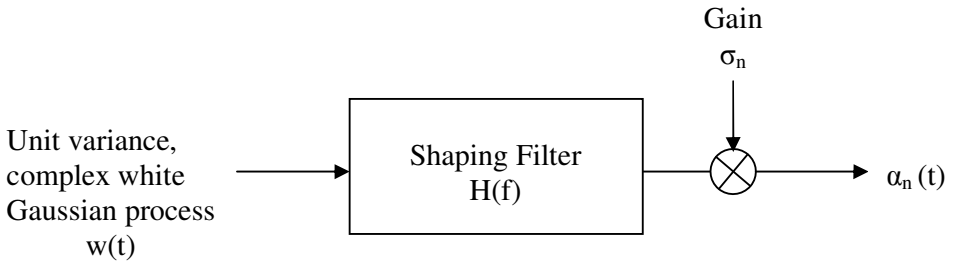

Figure 2.5 Adjustment of a tap weight.

An example of a Rayleigh fading envelope is provided for classical Doppler spectrum with f_d=150 Hz (v=90 km/h and f_c= 1800MHz) and f_d=42 Hz (v=50 km/h and f_c= 900MHz) in Figure 2.6 and Fig 2.7, respectively.

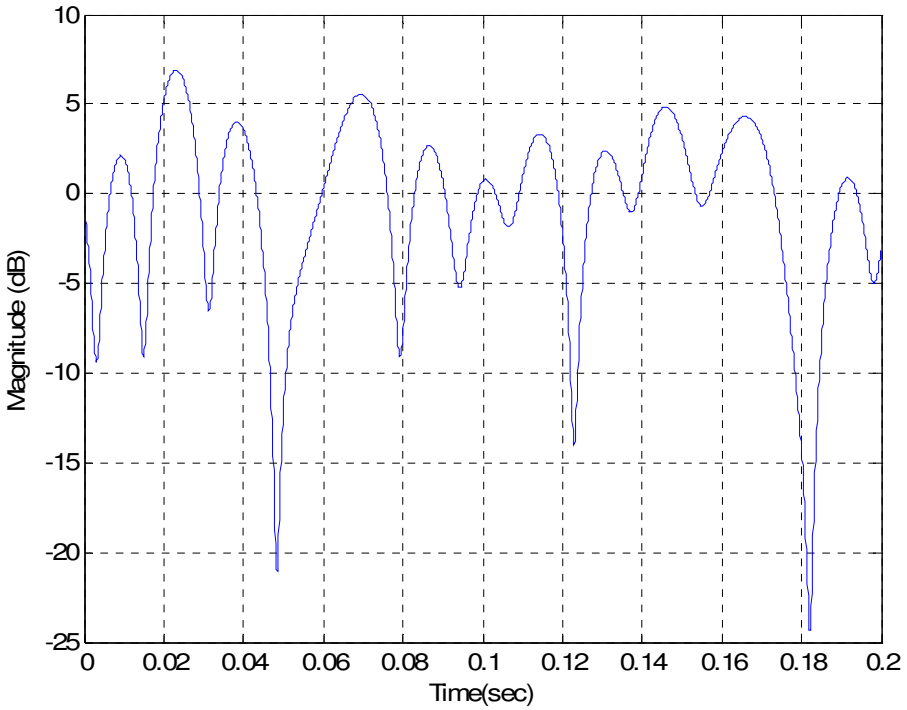

Figure 2.6 Rayleigh fading envelope $f_d = 42$ Hz.

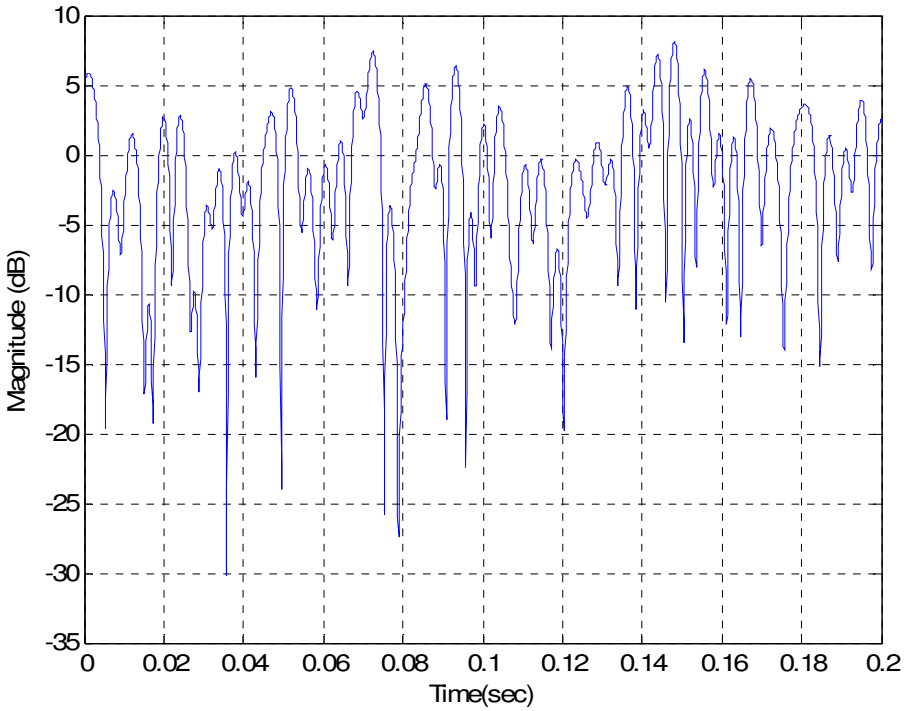

Figure 2.7 Rayleigh fading envelope $f_d = 150$ Hz.

2.3 MLSE RECEIVER FOR THE GMSK SIGNAL

2.3.1 The GMSK Signal

GMSK belongs to a family of the general class of continuous-phase modulation (i.e, binary CPM with h=0.5) (see Appendix A CPM Signals), which has special advantages of being quite narrow in its band with low adjacent channel interference and a constant amplitude envelope which allows the use of efficient amplifiers in the transmitters without special linearity requirements (class C amplifiers). Such amplifiers are especially inexpensive to manufacture and have high degree of efficiency [6].

As shown in Appendix A, the complex envelope of a GMSK signal is

$$s(t) = \sqrt{\frac{2E_s}{T}} e^{i(\theta + \phi(\alpha; t-\tau))}. \tag{2.17}$$

The phase of the modulated signal is:

$$\phi(\alpha; t) = 2\pi h \sum_i \alpha_i q(t - i\tau), \tag{2.18}$$

where the modulating index h is 0.5 and q(t) is the phase pulse of the modulator. Relation between q(t) and g(t) is given in (A.3). g(t) is the baseband shaping function given in (A.10) as

$$g(t) = \frac{1}{2T}\left[erf\left(-\frac{\sqrt{2}\pi B(t - T/2)}{\sqrt{\ln 2}} \right) + erf\left(-\frac{\sqrt{2}\pi B(t + T/2)}{\sqrt{\ln 2}} \right) \right]. \tag{2.19}$$

In the equation above, B is the 3 dB bandwidth of the filter and T is the bit duration.

In GSM, GMSK with a bandwidth data-rate product (BT) of 0.3 and a bit interval of 3.7μs (data rate of 270.83 Kbps) is used. The BT is a compromise between adequate BER and low level sidelobes necessary for satisfying the adjacent channel interference requirements. The baseband shaping pulse *g(t)* with a bandwidth data-rate product (BT) of 0.3 is shown in Figure 2.8.

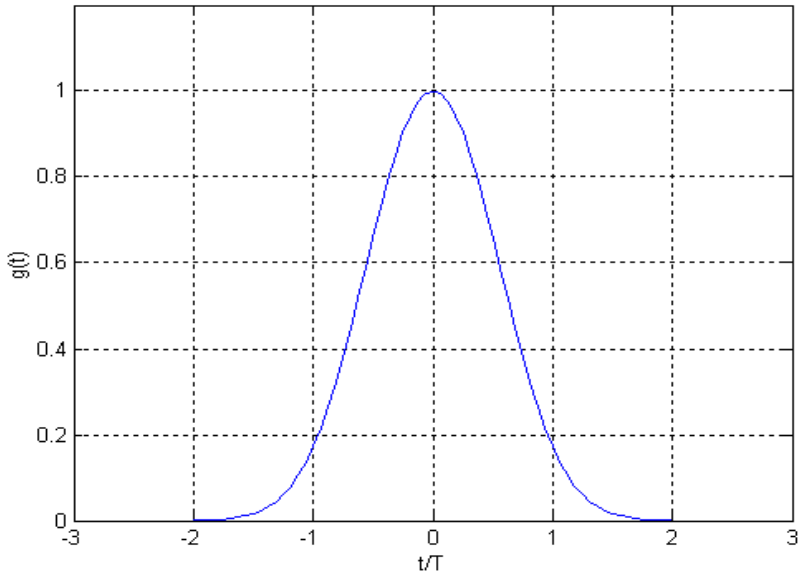

Figure 2.8 Baseband shaping pulse of *g(t)*.

According to the GSM standards, each data value d_i with a bit rate of R_b= 270.83 kbit/sec is precoded by the rule

$$d'_i = (d_i + d_{i-1}) \bmod 2, \quad d_i \in \{0,1\}. \tag{2.20}$$

The modulating data value $a_i \in \{\pm 1\}$ input to the modulator is obtained by the rule

$$a_i = 1 - 2\, d'_i . \tag{2.21}$$

Figure 2.9 summarizes the generation of GMSK signal.

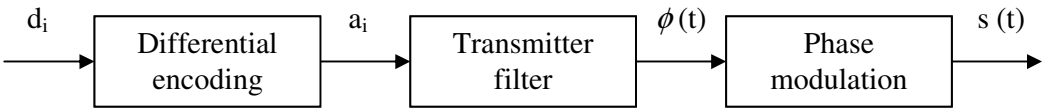

Figure 2.9 Generation of GMSK modulated signal.

Linear Approximation of GMSK

As mentioned before, GMSK modulation type belongs to the class of CPM. This modulation type is essentially nonlinear and hence classical MLSE algorithms for receiver side cannot work with the form of GMSK. It has been shown in the literature that every CPM signal can be represented approximately in linear quadrature amplitude modulation (QAM) signal format by adapting a suitable pulse shape [7].

In [7], [8] and [9], it is shown that complex envelope of a GMSK modulated signal, *s(t)* is exactly constructed by superposition of $N_c = 2^{L-1}$ impulses $C_{K.}$.

$$s(t) = \sum_{n=n_o}^{\infty} \sum_{K=0}^{N_c-1} \exp[j\pi h A_{K,n}] C_k(t - nT), \tag{2.22}$$

with

$$A_{K,n} = \sum_{i=n_0}^{n} d_i - \sum_{l=1}^{L-1} d_{n-l}.\alpha_{K,l}, \tag{2.23}$$

where $\alpha_{K,l}$'s are solved from

$$K = \sum_{l=1}^{L-1} 2^{l-1} \alpha_{K,l}, \qquad \alpha_{K,l} \in \{0,1\}, \qquad \text{K=0, 1,…. } N_c\text{-1.} \tag{2.24}$$

The data sequence is defined for $n \geq n_{o,}$ This representation can be used for all CPM signals For example the complex envelope of a MSK signal (L=1) can be written as follows:

$$s_{MSK} = \sum_{n=n_0}^{\infty} \left[\exp j\pi h \sum_{i=n_0}^{n} a_i \right] C_{0MSK}(t - nT), \tag{2.25}$$

where C_{0MSK} is a one half cycle sinusoidal with duration of two symbol period. (2.25) is the well known representation of MSK as OQPSK modulation.

For GMSK with L=3 the exact superposition is made by four impulses [10].

$$s_{GMSK} = \sum_{n=0}^{\infty} \left[\exp j\pi h \sum_{i=n_0}^{n} a_i \right] C_0(t - nT) + \sum_{n=n_0}^{\infty} \sum_{K=1}^{4} \left[\exp j\pi h A_{K,n} \right] C_K(t - nT), \tag{2.26}$$

$$= s^{lin}(t) + s^{nl}(t). \tag{2.27}$$

In [9], it is concluded that the GMSK modulated signal s_{GMSK} is the sum of a term $s^{lin}(t)$ and of a term $s^{nl}(t)$. Term $s^{lin}(t)$ can be interpreted as a linear mapping of the bit sequence a_i to waveforms. On the other hand, term $s^{nl}(t)$ causes the nonlinearity of the GMSK modulation with regard to the general definition of a linear modulation method. In Figure 2.10, the first two impulses C_0 and C_1 for GMSK are displayed. (See also Appendix B)

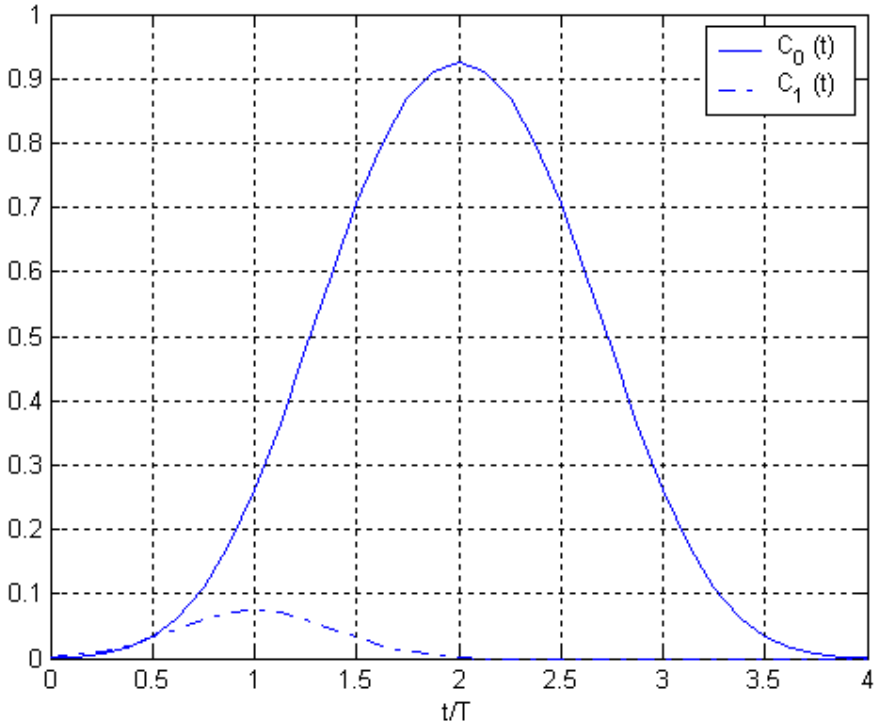

Figure 2.10 Comparison of C_0 (t) and C_1 (t).

Since C_0 has 99% of the signal energy [9], the following linear approximation is possible:

$$s_{GMSK} \approx s^{lin}(t) = s_{GMSK} = \sum_{n=n_0}^{\infty} z_n C_0 (t - nT), \tag{2.28}$$

where

$$z_n = \exp\left[j\pi h \sum_{i=n_0}^{n} a_i \right] \qquad \in \{-1, 1, -j, j\}, \tag{2.29}$$

are the symbols determined by the accumulated data stream a_i. Only $C_o(t)$ is used for pulse shaping. This approximation of the GMSK modulation is very similar to a PSK

or QAM signal. This approximated GMSK has the advantage that it can be realized with a ordinary I/Q-Modulator as used for PSK or QAM [9] , [10].

The GMSK modulated signal in baseband can be expressed as;

$$s_b(t) = \sum_{n=n_0}^{\infty} \exp\left(j\frac{\pi}{2}\sum_{i=n_0}^{n} a_i \right) C_0\left(t - nT\right), \tag{2.30}$$

where $C_0(t)$ denotes the real-valued pulse shaping function and a_i's $\in \{\pm 1\}$ are the input data bits to the modulator.

Effects of the Linear Approximation to GMSK:

The approximation of the GMSK causes a change of the scatter diagram and the power density spectrum.

The complex envelope of the approximate signal is not constant. In Figure 2.11, the scatter diagram of the approximated GMSK with BT=0.3 and BT=0.5 is shown. The disturbances are stronger for BT=0.3 than for BT=0.5. This is due to the fact that the GMSK with BT=0.5 is similar to the linear MSK and the linear approximation effect is small.

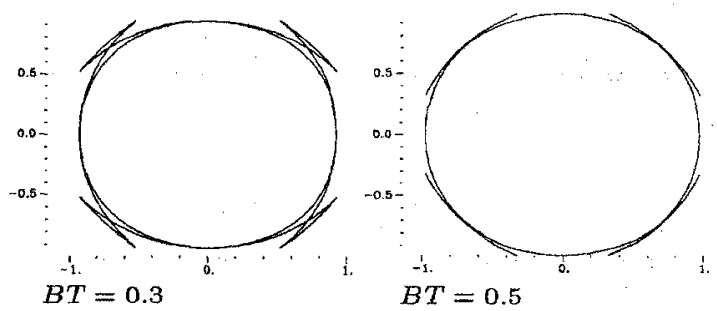

Figure 2.11 Complex envelope of approximated GMSK Signal [10].

In Figure 2.12 the PSD for linear approximated GMSK and exact GMSK are plotted. The approximate GMSK fits the requirements of the standardization at the PSD as good as the exact GMSK [10].

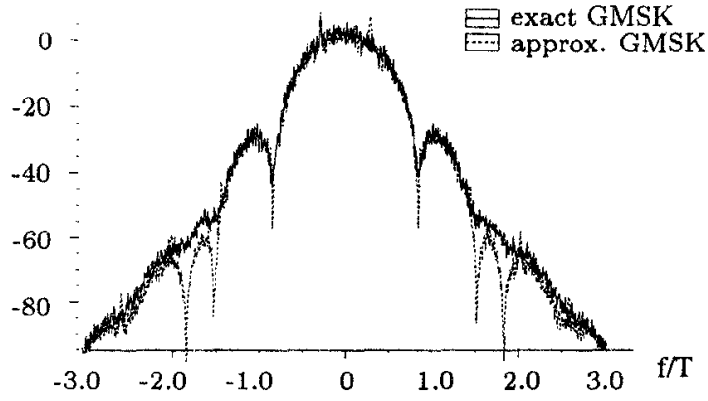

Figure 2.12 Power spectrum density of approximated and exact GMSK signal [10].

2.3.2 DEROTATION PROCEDURE

GMSK modulated baseband signal can be represented as;

$$s_b(t) = \sum_{n=n_0}^{\infty} \exp\left(j\frac{\pi}{2}\sum_{i=n_0}^{n} a_i \right) C_0\left(t - nT\right), \tag{2.31}$$

where a_i's are the input bits to the modulator and $C_0(t)$ is pulse shaping function as shown in Figure 2.10.

In GSM system, as mentioned before, the data to the modulator is obtained by the rule,

$$d'_i = (d_i + d_{i-1}) \bmod 2, \qquad d_i \in \{0,1\} \tag{2.32}$$

where d_i''s are original data bits.

$$a_i = 1 - 2\,d_i' \quad , \qquad a_i \in \{\pm 1\} \tag{2.33}$$

where a_i' s are inputs to the modulator.

The following procedure gives the same result as the above procedure;

$$c_i = 1 - 2\,d_i \ , \tag{2.34}$$

$$a_i = c_i\, c_{i-1} \ , \tag{2.35}$$

where c_i's $\in \{\pm 1\}$ are the original bits which are intended to be decoded in the receiver side.

GMSK modulated baseband signal is then given by

$$s_b(t) = \sum_{n=n_0}^{\infty} \exp\left(j\frac{\pi}{2}\sum_{i=n_0}^{n} c_i c_{i-1} \right) C_0\left(t - nT\right), \tag{2.36}$$

$$s_b(t) = \sum_{n=n_0}^{\infty} \prod_{i=n_0}^{n} \left(\exp j\frac{\pi}{2} c_i c_{i-1} \right) C_0\left(t - nT\right). \tag{2.37}$$

Because the term 'c_ic_{i-1}' is either -1 or +1, exp (j π/2 c_ic_{i-1}) is either exp (j π/2)= j or exp (- j π/2)= - j, thus exp (j π/2 c_ic_{i-1}) = j c_ic_{i-1}:

$$s_b(t) = \sum_{n=n_0}^{\infty} \prod_{i=n_0}^{n} j c_i c_{i-1} C_0\left(t - nT\right) \tag{2.38}$$

$$s_b(t) = \sum_{n=n_0}^{\infty} j^{n-n_0+1} \prod_{i=n_0}^{n} c_i c_{i-1} C_0\left(t - nT\right) \tag{2.39}$$

$$\prod_{i=n_0}^{n} c_i c_{i-1} = c_{n_0-1} c_n \prod_{i=n_0}^{n-1} c_i^{\,2} \ . \tag{2.40}$$

Because $c_i^{\,2}=1$ for all i,

$$\prod_{i=n_0}^{n} c_i c_{i-1} = c_{n_0-1} c_n \,, \tag{2.41}$$

$$s_b(t) = \sum_{n=n_0}^{\infty} j^{n-n_0+1} c_{n_0-1} c_n C_0 \left(t - nT\right). \tag{2.42}$$

$$s_b(t) = j^{-n_0+1} c_{n_0-1} \sum_{n=n_0}^{\infty} j^n c_n C_0 \left(t - nT\right) \tag{2.43}$$

Assuming the terms $c_{n_0-1}=1$ and $j^{(-n_0+1)}=1$ which are independent of n, it is convenient to express the GMSK modulated signal as follows;

$$s_b(t) = \sum_{n=n_0}^{\infty} j^n c_n C_0 \left(t - nT\right). \tag{2.44}$$

(2.44) can be expressed in discrete-time domain as follows;

$$s_{b_i} = \sum_{n=n_0}^{\infty} j^n c_n C_{0_{i-n}} \ . \tag{2.45}$$

The signal at the receiver will have passed through a frequency selective channel and a receiver filter in order to reject the out of band components. Let $g_R[n]$ denotes the discrete -time equivalent of receiver filter impulse response and $h_c[n]$ denotes the discrete-time equivalent of the channel impulse response. The received signal in baseband (absence of noise) can be expressed as follows;

$$r_i = \sum_{n=n_0}^{\infty} j^n c_n h_{i-n}\,, \tag{2.46}$$

where h[n]= C_0 [n] * h_c[n]* g_R[n] is the overall impulse response of the system from the output of the encoder to the detector input.

Equation (2.44) shows that the received signal samples can be obtained by convolving the input data with the overall system impulse response *h[n]* and then applying a $\pi/2$ phase rotation on a complex plane from symbol to symbol basis.

Phase rotation can be avoided by multiplying the received signal by the complex function q [i]=$(-j)^i$. The sequence q [n] is called *derotation sequence*.

Multiplying r [i] by the derotation sequence r´ [i] is obtained:

$$j^n = (-j)^{-n} = (-j)^{i-n}\,(-j)^{-i}, \tag{2.47}$$

$$r_i = (-j)^{-i} \sum_n c_n (-j)^{i-n} h_{i-n}\,, \tag{2.48}$$

$$r'[i] = r[i]\, q[i], \tag{2.49}$$

$$r_i' = \sum_n c_n (-j)^{i-n} h_{i-n}\,. \tag{2.50}$$

The derotated channel impulse response is $h'[i] = h[i].q[i] = h_i\,(-j)^i$:

$$h'_{i-n} = h_{i-n}\,(-j)^{i-n}. \tag{2.51}$$

Therefore,

$$r_i' = r_i q_i = \sum_n c_n h'_{i-n}\,. \tag{2.52}$$

By applying this derotation operation, the rotational structure of the signal is removed and a standard linear QAM structure model can be obtained.

2.3.3. MLSE Receiver, Viterbi Algorithm and Channel Identification

The classical MLSE receiver generally consists of an ML sequence estimator implemented by the Viterbi Algorithm. Viterbi algorithm uses the knowledge of channel characteristics and the received signal in order to find the most likely transmitted data sequence.

The form of r´ [i] given in equation (2.50) allows classical MLSE detection of the transmitted data sequence **c** by the use of Viterbi Algorithm. In the sequel, the subscripts indicating the derotation will be dropped for simplicity. The Viterbi Algorithm needs the knowledge of the channel impulse response (CIR).

A training sequence is used to produce an estimate of CIR at the receiver. This estimate is used in the demodulation process to equalize the effects of multipath propagation.

In GSM standards, the training sequence is placed at the centre of each burst to minimize the error in the information bits farthest from the training sequence. Consequently, the first section of the burst must be stored.

In GSM, the training sequence consists of a 16-bit sequence extended in both directions by copying the first five bits at the end of the sequence and the last five bits at the beginning. An example of training sequence is shown below:

0 0 1 0 0 1 0 1 1 1 0 0 0 0 1 0 **0 0 1 0 0** 1 0 1 1 1

Central 16 bits

The central 16 bits are chosen to have a highly peaked autocorrelation function, following GMSK modulation, and the repeated bits at either end ensure that the resulting channel estimate may be up to five bits wide before being corrupted by the information bits.

GSM specifications define eight different training sequences for using in a normal burst, each with low cross-correlation properties following GMSK modulation. Consider the case of two similar simultaneous signals arriving at the receiver at the same time one of them is interference. If their training sequences are identical, there is no way to distinguish the contribution of each to the received signal. When training sequences are different and are as little correlated as possible, the situation is much clearer.

Each training sequence is described by a training sequence code (TSC). A list of the TSC is given in Table 2.1.

Table 2.1 Training sequence codes.

Training sequence code (TSC)	Training sequence bits
0	0,0,1,0,0,1,0,1,1,1,0,0,0,0,1,0,0,01,0,0, 1,0,1,1,1
1	0,0,1,0,1,1,0,1,1,1,0,1,1,1,1,0,0,0,1,0,1,1,0,1,1,1
2	0,1,0,0,0,0,1,1,1,0,1,1,1,0,1,0,0,1,0,0,0,0,0,1,1,1,0
3	0,1,0,0,0,1,1,1,1,0,1,1,0,1,0,0,0,1,0,0,0,1,1,1,1,0
4	0,0,0,1,1,0,1,0,1,1,1,0,0,1,0,0,0,0,0,0,1,1,0,1,0,1,1
5	0,1,0,0,1,1,1,0,1,0,1,1,0,0,0,0,0,0,1,0,0,1,1,1,0,1,0
6	1,0,1,0,0,1,1,1,1,1,0,1,1,0,0,0,1,0,1,0,0,1,1,1,1,1
7	1,1,1,0,1,1,1,1,0,0,0,1,0,0,1,0,1,1,1,0,1,1,1,1,0,0

Figure 2.13 shows the autocorrelation function of one of these eight training sequences calculated between the central 16 bits and the whole 26-bit sequence. The

difference between the central correlation peak value and those five on each side is 4 for all eight sequences.

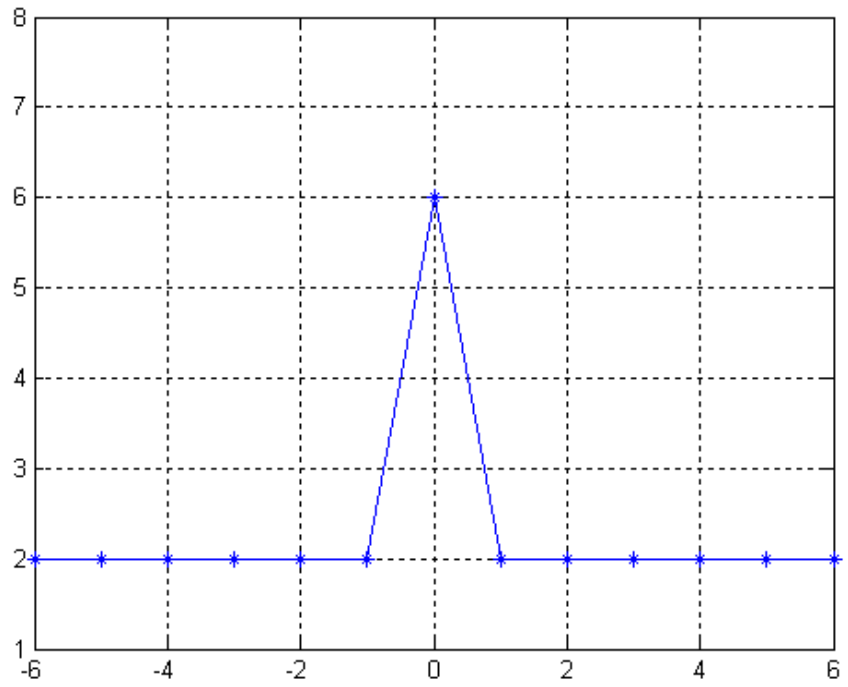

Figure 2.13 Correlation function between the central 16 bits and the whole training sequence.

The method for estimating the CIR is based on correlating the central 16 samples of received midamble with the original midamble word as follows [11];

$$R_{av}(i) = \frac{1}{16}\sum_{n=5}^{20} v_n c_{n-i} \tag{2.53}$$

where v_n's, $5 \le n \le 20$ are central of the received midamble and c_n' s, $0 \le n \le 25$ are the original midamble bits which are known to receiver.

The performance of the MLSE receiver is dependent on the available estimate of the channel impulse response. If the training sequence is placed in front of the burst channel impulse response will be obtained by the same correlation method, but performance of estimating CIR is not as good as the case of the training sequence is placed in the centre of each burst. [12].

The received signal without noise can be expressed as

$$r_i = \sum_n c_n h_{i-n} \,. \tag{2.54}$$

With the assumption that the function h(t) is known, the received signal for each possible sequence may be reconstructed. The reconstructed complex signal for the m^{th} sequence is denoted as

$$s_b^m[i] = \sum_{n=0}^{\infty} j^n c^m[n] c_0[i-n]. \tag{2.55}$$

The MLSE algorithm attempts to find the transmitted sequence (c^m) that maximizes the log likelihood function [3].

The one among all the possible vectors **c** which maximizes LLF is the direct solution of the maximization problem. But this is not an efficient solution method especially when **c** gets larger. In order to reduce computational load Viterbi algorithm can be used.

The proposed symbol synchronizer presented in section 4.3 depends on the performance of Viterbi algorithm. Throughout the study, the perfect estimation of the channel estimation is assumed and tentative decisions from Viterbi algorithm are assumed to be error free.

The general block diagram of the system model consists of GMSK modulator, fading channel and MLSE receiver is shown in Figure 2.14

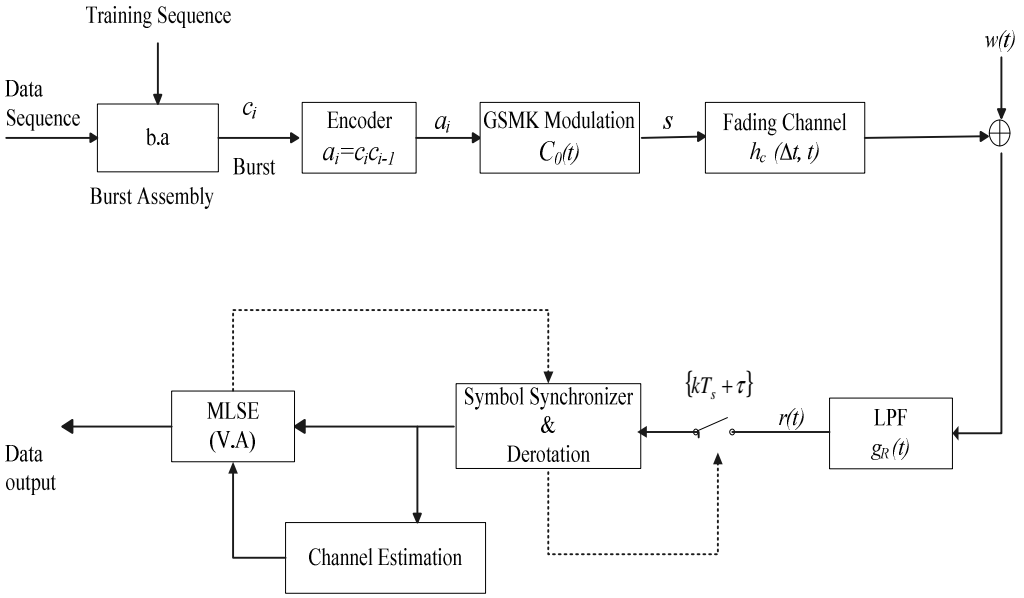

Figure 2.14 General block diagram of GMSK system model.

CHAPTER 3

SYMBOL SYNCHRONIZATION REVIEW

3.1 INTRODUCTION

Timing recovery is one of the most critical functions that are performed at the receiver of a synchronous digital communication system. The receiver must know not only the frequency at which the outputs of the demodulators are sampled, but also where to take the samples within each symbol interval.

In this chapter, firstly the definition of symbol synchronization is presented. Secondly, a review of symbol timing recovery (STR) methods is given to highlight the attributes. In the context of this review, a brief history of timing recovery with some applications on MSK signals is included. Finally, the maximum likelihood estimation of the timing recovery is presented.

3.2 SYMBOL TIMING RECOVERY

In a digital communication system, the output of the baseband filter (a matched filter) must be sampled periodically at the precise sampling time instants that minimize the detector error probability. The process of extracting the clock signal for determining the accurate locations of the maximum eye openings for reliable

detection is usually called symbol synchronization or symbol timing recovery (STR). A system that is able to estimate such locations is called a timing (or) clock synchronizer.

Figure 3.1 illustrates the block diagram of a typical baseband receiver model with a channel introducing an arbitrary delay τ. The received signal is composed of signal plus noise:

$$r(t)=s(t-\tau)+w(t), \tag{3.1}$$

where w(t) is a noise process. The received waveform is first filtered to remove the out-of-band noise and then sampled at T-spaced instants, tk = kT + τ, where τ is the timing epoch that accounts for the propagation time of the signal from the transmitter to the receiver.

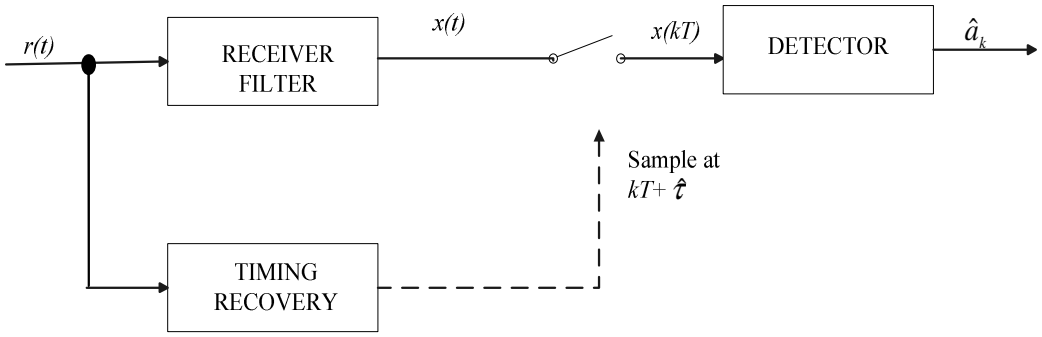

Figure 3.1 Typical block diagram of a baseband receiver.

The task of the timing recovery function, as stated, is to sample at the optimum sampling instants, which amounts to the maximum eye opening at the output of the receiver filter. This will ensure that the samples passed to the remaining receiver processes, including data detection, have the maximum available average

signal-to-noise ratio (SNR) and hence a bit error rate (BER) as close as possible to optimum.

3.2.1 Existing STR Schemes

The books written by Meyr and Ascheid [13], Meyr, Moeneclaey and Fechtel [14], and Mengali and D'Andrea [15] are excellent references in the symbol synchronization literature.

Existing symbol synchronizers are modeled with analog or digital methods. Due to a time shift between transmitter and receiver, samples at $t=kT+\tau$ are required. In analog methods continuous- time waveforms are operated on. In digital method, in order to perform the recovery of the timing epoch signal samples taken at a suitable rate are processed. Main emphasis is given to digital timing recovery in this section.

From the operating principle point of view, two categories of synchronizers are distinguished, i.e. error tracking (or feed back, or closed loop) synchronizers and feedforward (or open loop) synchronizers. Feedback configuration and Feedforward configuration are shown in Figure 3.2 and 3.3.

In both configurations anti alias filter (AAF) limits the bandwidth of the received waveform. Sampling is controlled by a fixed clock whose ticks are not locked to the incoming data. The bulk of the pulse shaping is performed in the matched filter whose location is not necessarily that shown in the figures. The MF may be moved inside the loop in Figure 3.2 or it may be shifted so as to have a common input with the timing estimator in Figure 3.3 [15].

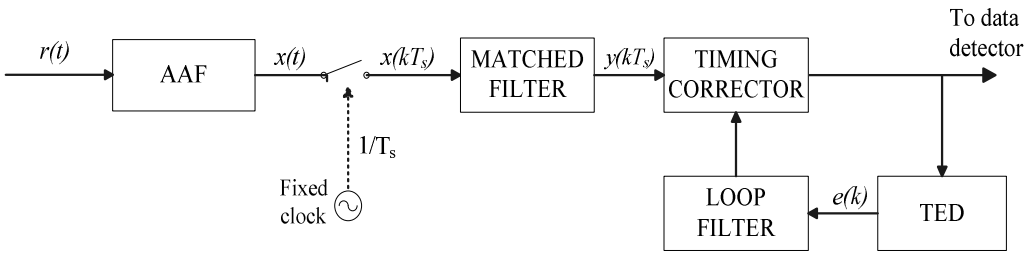

Figure 3.2 Feedback configuration.

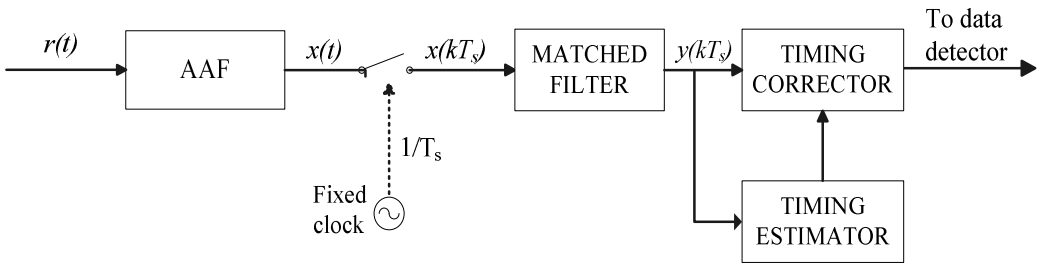

Figure 3.3 Feedforward Configuration.

Timing correction is akin to the operation of a voltage controllable delay line and produces synchronized samples to be used for decision and synchronization purposes. Timing correction is generally performed with interpolators with the desired interpolation times $\{t_k\}$.

In feedback configuration timing corrector feeds a timing error detector (TED) whose purpose is to generate an error signal e(k) proportional to the difference between τ and its current estimate. The error signal is then exploited to recursively update the timing estimates. The error signal is then filtered to reduce the

variance of the timing error and the output is used to recursively update the timing estimates.

On the other hand, feedforward methods derive an estimate of the timing epoch by applying a non-linear process to the received signal samples. The estimate is used to adjust the sample timing to the optimum location.

In a fully digital implementation, sampling is not locked to the incoming pulses. This is referred as non-synchronous sampling. Also sampling can be made synchronous by exploiting some error signal to adjust the timing phase of a number controlled oscillator (NCO). As shown in Figure 3.4 the sampler is commanded by the NCO pulses at times $\{ t_n\}$. The analog MF in the Figure 3.4 may be replaced by a digital MF inside the loop.

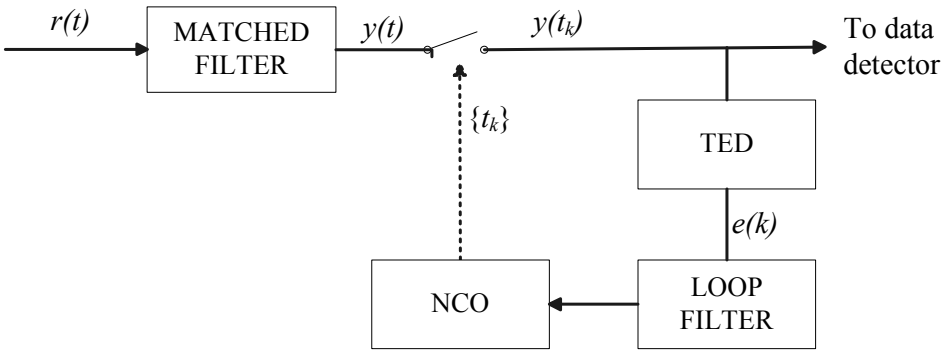

Figure 3.4 Synchronous sampling.

When a synchronizer makes use of the receiver's decisions about the transmitted data symbols for producing a timing estimate, the synchronizer is called decision-directed (DD) or data-aided (DA). In the literature, DA timing recovery is generally referred to estimation of the timing epoch by using some preamble known to the receiver.

When a synchronizer determines the timing phase error without using knowledge of the transmitted data values, the synchronizer is called non-decision-directed (NDD) or non-data aided, (NDA).

Next section gives the details of the research on symbol synchronization in CPM signals.

3.2.2 Symbol Synchronization in CPM Signals

MSK and GMSK are subsets of the continuous phase modulation (CPM) schemes as explained in Appendix A. This section gives a history of timing recovery with CPM signals especially with MSK and GMSK signals.

Symbol timing recovery for CPM signals has been first discussed by de Buda [16], specifically for minimum shift keying (MSK), where a nonlinearity is used to generate tones at the clock frequency. This algorithm was further analyzed in some papers and in [17] it has been shown that it can be used for any CPM signal. The problem with these Buda-like [18] synchronizers is their poor performance with the smoothed frequency pulses.

A decision-directed (DD) algorithm based on the maximum likelihood (ML) techniques is proposed in [19] using MSK modulation. The method provides the joint ML estimation of carrier phase, timing epoch and data, but suffers from spurious locks in the maximization of the likelihood function.

In order to solve the problems related with the mentioned algorithms some NDA structures are developed. In [20],[21],[22] feedforward NDA algorithms are discussed. Two of these methods, proposed by Mehlan, Chen and Meyr [20] and Lambrette and Meyr [21], recover the clock signal in an ad hoc manner by passing the received signal samples through a nonlinearity and a digital filter. The algorithm

behind this ad-hoc scheme obtained specifically for pure MSK and not applicable to any other CPM format. In a different approach, [22], the non-data-aided recovery is obtained by applying maximum likelihood methods. Although it is simple and seems suitable for burst mode transmission the algorithm is obtained under the assumption of low SNR. This results in the deviation from the desired performance even in the moderate SNR values.

Although, it is widely believed that conventional clock synchronizers can be used even with fading channels, a closer look at the question may be worthwhile. In [20] and [23], the effects of a flat fading channel are taken in consideration with the symbol synchronizer employing nonlinearity and filtering in a feedforward manner. Also, the effect of frequency- selective channels is tested in [20], and a dramatic degradation is found in the bit error rate.

3.3 MAXIMUM LIKELIHOOD TIMING ESTIMATION

It is widely recognized that maximum likelihood (ML) estimation techniques offer a systematic and conceptually simple guide to the solution of synchronization problems and they provide optimum or nearly optimum solutions.

In this section the framework for maximum likelihood symbol timing recovery is established since most of the algorithms have been discovered by application of the ML estimation [24]. This is also the case for the proposed algorithm given in Section 4.3. The general formulation of the ML timing estimation is discussed in detail in [15] and [25].

Considering the baseband equivalent of the bandpass signal, the received signal in (3.1) can be described as

$$r(t) = s_l(t, \tau) + w(t)\,, \tag{3.2}$$

where τ represents an arbitrary delay introduced by the channel to the transmitted signal $s_l(t)$. The notation $s_l(t,\tau)$ is adopted to stress the dependence of the signal on the timing epoch. $w(t)$ is white Gaussian noise with spectral height $N_0/2$.

The ultimate goal of a symbol synchronizer is to estimate the most likely value of the timing epoch. This is accomplished when synchronizer maximizes the aposteriori probability for all values of τ:

$$\hat{\tau}_{MAP} = \arg\max_{\tau} \left\{ p_{\tau|r}(\tau \mid r(t)) \right\}, \tag{3.3}$$

given the observed signal *r(t)* [26].

ML estimation requires the determination of the signal $r(t)$ which maximizes the conditional probability density function $p_{r\backslash s_l}(r(t)\backslash s_l(t,\tau))$, that is, the most likely signal, $s_l(t,\tau)$, which produces the received signal, $r(t)$, over a specific observation period T_o.

We can rewrite the *a posteriori* probability using Bayes' theorem:

$$p_{\tau|r}(\tau \mid r(t)) = p_{r|\tau}(r(t)|\tau)\frac{p_\tau(\tau)}{p_r(r(t))}, \tag{3.4}$$

where $p_r(r(t))$ describes the probability that $r(t)$ was received, and $p_\tau(\tau)$ describes the probability that $s_l(t,\tau)$ was transmitted with a delay of τ. In this case $p_\tau(\tau)$ is a constant assuming the time delay has a uniform pdf over the interval [0,T]. In addition, $p_r(r(t))$ is simply a normalized constant.

Let $\bar{r}$, $\bar{s}_l(\tau)$ and $\bar{w}$ be the vector representations of $r(t)$, $s_l(t,\tau)$ and $w(t)$ over a complete orthonormal set $\{\phi_i(t)\}_{i=1}^{K}$. Then, the i-th component of $\bar{r}$ is given by [26] as

$$r_i = \int_{T_0} r(t)\phi_i(t)dt \,, \tag{3.5}$$

where T_0 devotes the observation interval. Similarly,

$$s_{li}(\tau) = \int_{T_0} s_l(t,\tau)\phi_i(t)dt \,, \tag{3.6}$$

$$w_i = \int_{T_0} w(t)\phi_i(t)dt \,, \tag{3.7}$$

The standard form of the pdf for the sum of a known signal and AWGN, is

$$p_{r|\tau}(r_i \mid \tau) = \frac{1}{\sqrt{\pi N_0}} \exp\left[\frac{-(r_i - s_{li}(\tau))^2}{N_0}\right], \tag{3.8}$$

As the additive noise is considered to be white, the observations of noise, w_i's, are independent, that is,

$$E\{w_i w_j\} = \frac{N_0}{2}\delta(i-j) \,, \tag{3.9}$$

Hence, the pdf may be expanded over *K* components by taking the product of the pdfs for the individual sample observations and leads to the desired result

$$p_{r|\tau}(\bar{r} \mid \tau) = \frac{1}{\left(\sqrt{\pi N_0}\right)^K} \prod_{i=1}^{K} \exp\left[\frac{-(r_i - s_{li}(\tau))^2}{N_0}\right], \tag{3.10}$$

within the observation interval T_0. To simplify the likelihood function the natural logarithm may be taken, which after some rearrangement, results in

$$\ln\left[p_{r|\tau}(\bar{r} \mid \tau)\right] = -\frac{1}{N_0} \sum_{i=1}^{K} (r_i - s_{li}(\tau))^2 + C_K \,, \tag{3.11}$$

where

$$C_K = \ln\left[\frac{1}{\left(\sqrt{\pi N_0}\right)^K}\right], \tag{3.12}$$

Equation (3.11) can be converted to the continuous time domain form by dropping the constant C_K as it is independent of the time delay and taking the limit as $K \rightarrow \infty$. Then, the result is

$$\Lambda_L(\bar{r} \mid \tau) = -\frac{1}{N_0} \int_{T_0} (r(t) - s_l(t,\tau))^2 dt \,, \tag{3.13}$$

where $\Lambda_L(\bar{r} \mid \tau)$ is the continuous time log likelihood function (LLF). The squared term within the integral is a measure of the distance between the received and reference signals. Only the cross-correlation term in (3.13) contains useful information regarding the time epoch. $r^2(t)$ is independent of τ, and the $s_l^2(t,\tau)$ term is simply the power of the transmitted signal during the observation interval T_0. Consequently, the most likely timing offset $\hat{\tau}$ can be expressed as the value of τ which maximizes

$$\Lambda_L(\bar{r} \mid \tau) = \frac{2}{N_0} \int_{T_0} r(t) s_l(t, \tau) dt + const\,, \tag{3.14}$$

that is,

$$\hat{\tau} = \arg\max_{\tau} \left\{ \Lambda_L(\bar{r} \mid \tau) \right\} = \arg\max_{\tau} \left\{ \frac{2}{N_0} \int_{T_0} r(t) s_l(t, \tau) dt \right\}. \tag{3.15}$$

The constant term is not included in (3.15), as it does not affect the maximization process. The synchronization scheme investigated in this thesis is based on the final expression and the details are provided in the next chapter.

CHAPTER 4

A DD STR BASED ON MATCHED FILTERING FOR GMSK SIGNALS

4.1 INTRODUCTION

Synchronizer is one of the most critical receiver functions and comparison of the performance of the synchronizers with a reference bound is an important point. Therefore, this chapter starts with the presentation of Modified Cramer Rao Bound (MCRB) and Mazo Criterion. Modified Cramer Rao Bound (MCRB) is commonly used under AWGN channel as a bound. In [1], minimum squared ISI (msISI) criterion and Mazo criterion are presented as an optimum value criteria for considering fading channel effects. As a result similarity between msISI criterion and Mazo criterion is emphasized. In this study, the criterion proposed by Mazo [28] is used as optimum timing phase criteria under Rayleigh fading channel.

Transmission over frequency selective fading channel necessitates specifically designed synchronizer structures and algorithms that are different from those for static channel. In the second part of this chapter, the proposed timing recovery scheme based on the method of ML estimation of the timing epoch in [1] is reviewed. The proposed timing recovery scheme does not employ any feedback loop so that it does not suffer from hang-up problems which are common in feedback schemes. Correlation (matched filter) method is used for the recovery of the timing epoch. In order to determine fractional delays correlation between the received signal and the reference samples is interpolated and an iterative maximum search is

performed. Finally a discussion on the performance of the proposed timing recovery scheme for GMSK is given.

4.2. CRITERIA FOR TIMING PHASE

4.2.1. Modified Cramer Rao Bound

In the literature considerable number of technical papers makes use of the modified Cramer–Rao bounds (MCRB's) for timing estimation as benchmarks. Cramer-Rao bound is a lower limit to the variance of any unbiased estimator.

$$Var\{\hat{\tau}(\bar{r}) - \tau\} \geq CRB(\tau), \tag{4.1}$$

Let $\hat{\tau}(\bar{r})$ be estimation of τ. $\hat{\tau}(\bar{r})$ depends on the observation $\bar{r}$.

Cramer-Rao bound is expressed as

$$CRB(\tau) \stackrel{\Delta}{=} -\frac{1}{E_r\left\{\dfrac{\partial^2 \ln \Lambda(\bar{r} \mid \tau)}{\partial \tau^2}\right\}}, \tag{4.2}$$

$$= \frac{1}{E_r\left\{\left[\dfrac{\partial \ln \Lambda(\bar{r} \mid \tau)}{\partial \tau}\right]^2\right\}}.$$

Unfortunately, application of the bound to synchronization problems leads to serious mathematical difficulties. MCRB's are much easier to employ, but are loose than true CRB's. The relation between the bounds is

$$Var\{\hat{\tau}(\bar{r}) - \tau\} \geq CRB(\tau) \geq MCRB(\tau). \tag{4.3}$$

In Figure 4.1, $CRB(\tau)$ and $MCRB(\tau)$ are qualitatively drawn as afunction of the signal to noise ratio E_s / N_o.

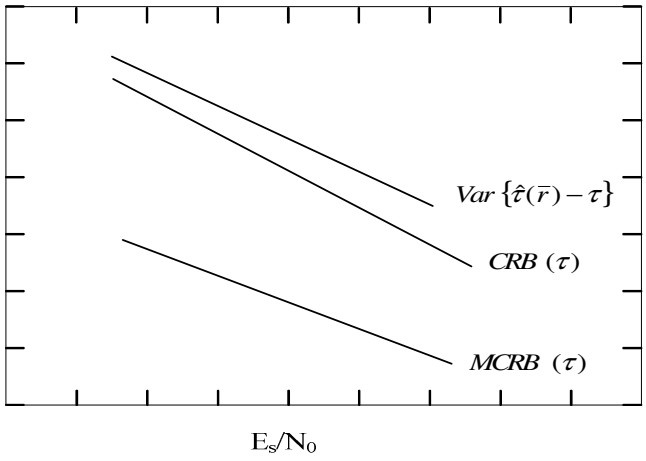

Figure 4.1 Error variance, $CRB(\tau)$ and $MCRB(\tau)$ [15].

Modified Cramer Rao bound and Cramer Rao bound will be equal when unwanted parameters are perfectly known or there are no unknown parameters.

In [15], Cramer-Rao and Modified Cramer-Rao bounds are described in detail. $MCRB(\tau)$ for CPM is given in as

$$\frac{1}{T^2} \text{x}\, MCRB(\tau) = \frac{1}{8\pi^2 \zeta L_0} \frac{1}{E_s / N_0}, \tag{4.4}$$

where $\zeta \overset{\Delta}{=} h^2 T \int_{-\infty}^{\infty} g^2(t)dt$, $g(t)$ is the shaping pulse and L_0 is the observation interval in terms of the symbol period.

For MSK:

$$g(t)=\begin{cases}\dfrac{1}{2T}, & 0\le t\le T,\\ 0, & elsewhere,\end{cases} \tag{4.5}$$

Thus (4.4) reduces to a simple form

$$\frac{1}{T^2}\,\mathrm{x}\,MCRB(\tau)=\frac{2}{\pi^2 L_0}\frac{1}{E_s/N_0}, \tag{4.6}$$

To find $MCRB(\tau)$ for GMSK, equation (4.4) is used with pulse shaping

$$g(t)=\frac{1}{2T}\left[erf\left(-\frac{\sqrt{2}\pi B(t-T/2)}{\sqrt{\ln 2}}\right)+erf\left(-\frac{\sqrt{2}\pi B(t+T/2)}{\sqrt{\ln 2}}\right)\right]. \tag{4.7}$$

4.2.2 Mazo Criterion

In this criterion, optimum timing phase is defined as the one which results in the least MMSE, at the output of an equalizer. For most transmission systems the bandwidth is greater than 1/2T where T is the symbol period. Therefore, when it is sampled at a rate 1/T, the sampling phase will change the equivalent system response by canceling or augmenting the aliased components. It has been shown by Mazo [28] that for a system consisting of a channel, a sampler and a forward linear equalizer the optimum timing is found by maximizing the equivalent channel magnitude response at the frequency 1/2T, i.e., at the Nyquist band edge.

The received signal samples at time instants t = kT + τ, can be re-expressed in the absence of noise by

$$r_k(\tau)=\sum_n h_n(\tau)a_{k-n}, \tag{4.8}$$

where the notation $h_n(\tau) = h(nT + \tau)$ is used. These samples are related to their discrete Fourier transform as,

$$h_n(\tau) = \int_{-\infty}^{\infty} H_{eq}(f,\tau) e^{j2\pi fnT} df \,, \tag{4.9}$$

where

$$H_{eq}(f,\tau) = \sum_n H(f + n/T) e^{-j2\pi(f+n/T)\tau} \,, \tag{4.10}$$

is the equivalent channel response taking folding effects into account due to sampling.

The exponential term in (4.10) reflects the effect of the timing phase. If the excess bandwidth of the sampled received signal is assumed to be less than 100%, then

$$H_{eq}(1/2T,\tau) = H(1/2T) e^{-j\pi\tau/T} + H(-1/2T) e^{j\pi\tau/T} \,, \tag{4.11}$$

According to the criterion proposed by Mazo [28], the optimum timing phase is defined as τ_{opt} that maximizes the cost function $\left|H_{eq}(1/2T,\tau)\right|^2$ and is approximately given by

$$\tau_{opt} = \frac{T}{2\pi}\left[\arg(H(1/2T)) - \arg(H(-1/2T))\right] + kT \,, \tag{4.12}$$

where *k* is any integer.

The equation derived by Mazo is nothing but the slope of the phase response between the frequencies *{-1/2T, 1/2T}*. Correspondingly, the timing phase behaviour

given with this relation can be characterized by the slope of the phase response in a way given in the following formula:

$$\tau = \frac{1}{2\pi(f_1 - f_2)}\left[\arg(H(f_1)) - \arg(H(f_2))\right] + kT\,, \tag{4.13}$$

with $f_1 = -f_2 = 1/2T$.

This result directly gives the delay for linear phase systems, and in a sense may show the general tendency of the time-variant channel.

Figure 4.2 and 4.3 show some examples for the timing values obtained by equation (4.13) for different f_1 and f_2. In Figure 4.2, the variations of the timing phase are obtained for a multipath channel which corresponds to a variation with a mobile speed of 50 km/h and a carrier frequency of 900 MHz. In Figure 4.3 a faster channel exists. The variations of the timing phase are drawn for a multipath channel which corresponds to a variation with a mobile speed of 90 km/h and a carrier frequency of 1800MHz.

In Figure 4.2 and Figure 4.3 the curves coincide at some specific interval and give the same delay. At other instants, the values of timing phase differ for different frequency pairs. Of course, this depends on the channel characteristics, but gives some information about the channel variations and the effects on optimum timing phase.

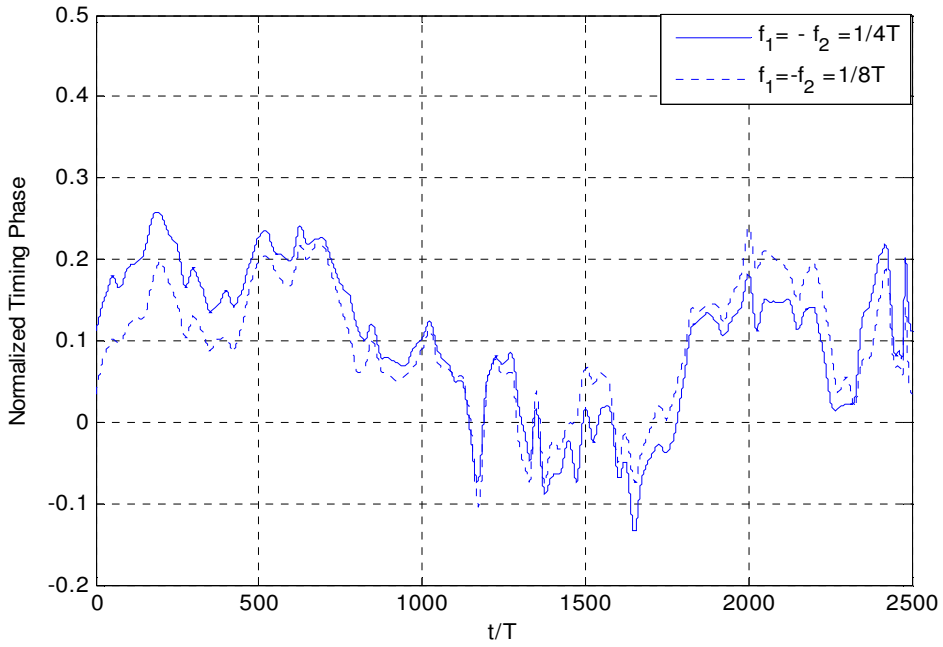

Figure 4.2 Normalized timing phase obtained from Mazo criterion (v=50 km/h, f_c=900 MHz, f_d = 42Hz).

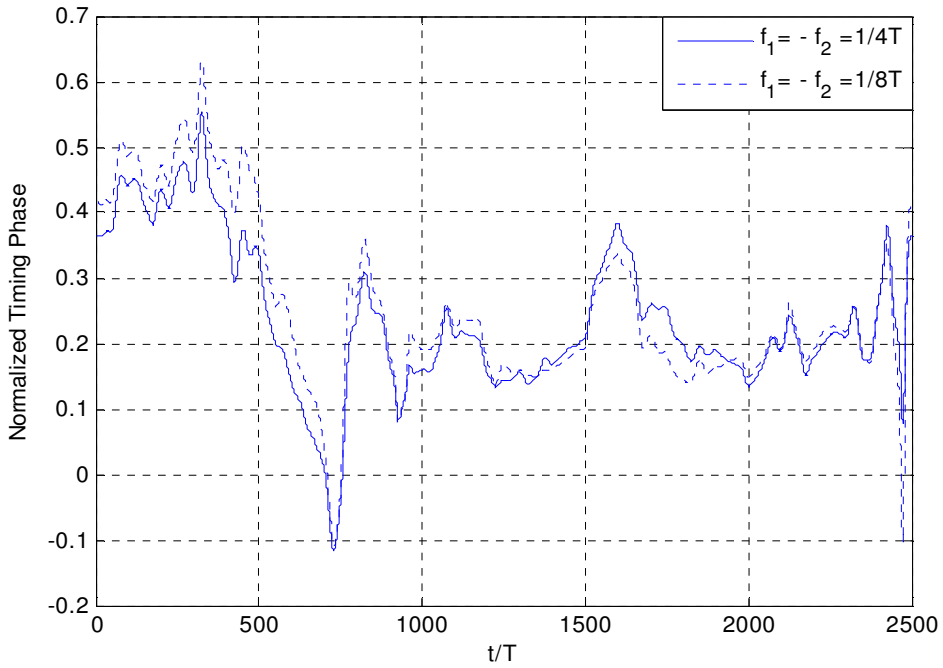

Figure 4.3 Normalized timing phase obtained from Mazo criterion (v=90 km/h, f_c=1800 MHz, f_d= 150Hz).

4.3. PROPOSED DD STR FOR GMSK SIGNALS

A decision-directed timing recovery scheme was proposed in [1] and [2]. It simply employs a correlation (matched filter) method based on the maximum likelihood (ML) estimation of the timing epoch. For determining the fractional delays, interpolation and an iterative maximum search algorithm are used.

4.3.1. Correlation (Matched Filter) Method

In the literature, a large number of algorithms that use several versions of ML estimators exist. The notion behind the proposed symbol timing estimation algorithm depends on the theory of maximum likelihood (ML) estimation. The proposed symbol timing estimator does not give the estimates of the timing offset explicitly. It is based on the determination of the maximum value of the log likelihood function as a function of τ, i.e.,

$$\hat{\tau} = \arg\max_{\tau}\{\Lambda_L(\tau)\}, \tag{4.14}$$

Let us rewrite the likelihood function (3.14) obtained in Section 3.3:

$$\Lambda_L(\tau) = \frac{2}{N_0}\int_{T_0} r(t)s_l(t-\tau)dt\,, \tag{4.15}$$

The integral in (4.15) is just a convolution operation. The likelihood function is simply the output of a filter with impulse response $s_l(-t)$ and input $r(t)$ over the observation interval T_0. Then, the estimate of the symbol timing offset may be obtained by finding the timing instant which corresponds to the maximum of the output of the cross-correlation between the received and the reference signal samples. The correlation function can be expressed as

$$R(t) = \int_{T_0} r(u)s(u-t)du \,, \tag{4.16}$$

and the proper sampling instant is given by

$$t_{samp} = \arg\max_{t} R(t) \,, \tag{4.17}$$

The correlation function can also be viewed as the output of a filter matched to reference signal when the input is the received signal.

The proposed synchronizer has two main modes: First one is the acquisition mode and the other one is the tracking mode. In the acquisition mode of the synchronizer a training sequence is employed. Training sequences can be selected from Table 2.1. The initial adjustment of the clock is accomplished by finding the timing instant which corresponds to the maximum of the output of the cross-correlation between the received and the transmitted signal samples which is formed by the training sequence.

After the initial adjustment of the clock, in the tracking mode, the channel variations are tracked in a decision-directed manner using the decisions coming from the MLSE receiver (Viterbi algorithm). These decisions are referred to as tentative decisions. The tentative decisions are used to form a filter matched to the GMSK waveform. The correlation function defined in (4.16) is obtained from the output of the matched filter with its input being the received signal. The timing epoch is estimated by determination of the instant corresponding to the maximum of the matched filter output. Estimated timing epoch is in terms of sampling time, in order to obtain fractional timing epoch interpolation and an iterative maximum search algorithm are used.

As a summary the general flow of the proposed timing recovery process is shown in Figure 4.4. The received samples are first taken into the data buffer and

then passed through the matched filter. Matched filter is obtained from the training sequence in the acquisition mode or the tentative decisions in the acquisition mode. Next, precise timing information is obtained by the iterative maximum search process using interpolator and Bisection Method. In the following sections interpolation and an iterative maximum search process are explained.

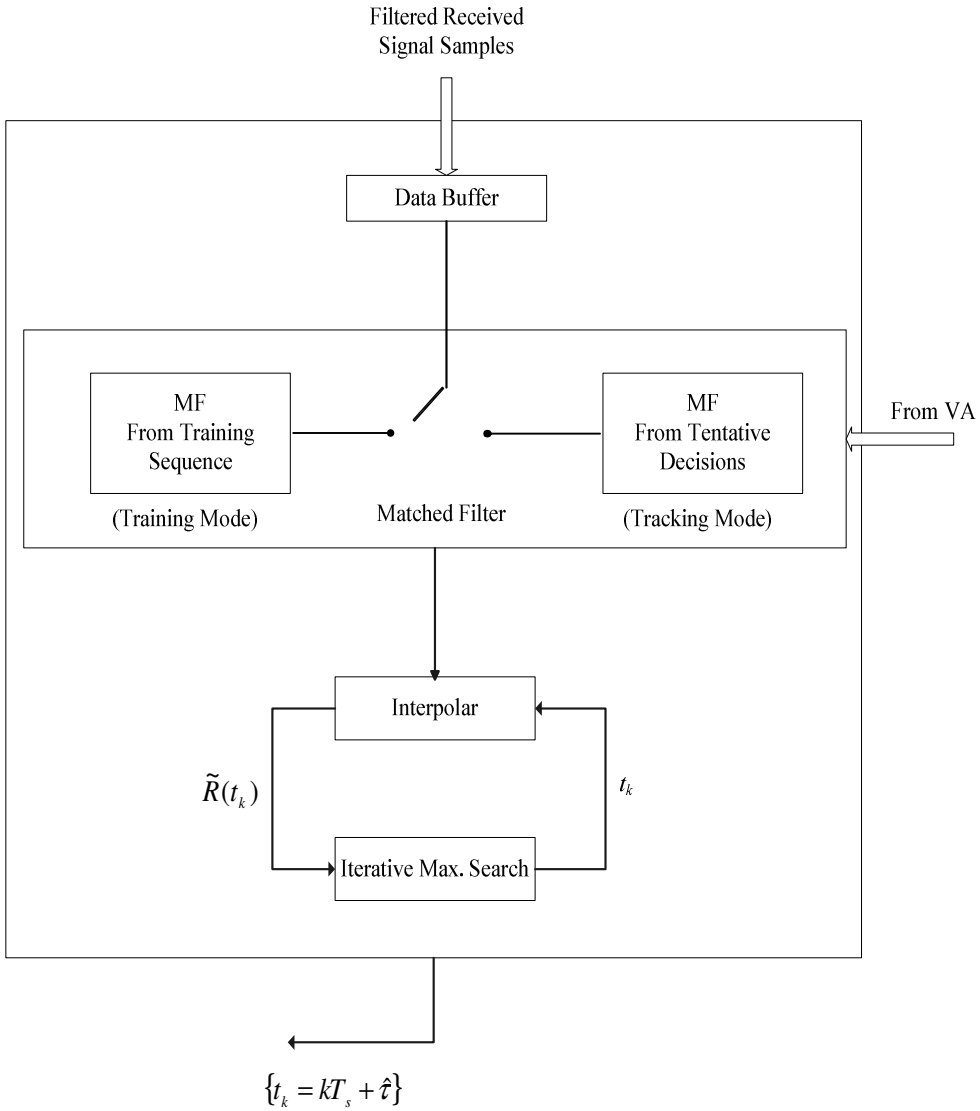

Figure 4.4 General flow in the proposed timing recovery scheme.

4.3.2. Iterative Maximum Search

In determining the maximum of the correlation function, a simple and satisfactory iterative process based on Bisection Method is employed. The iteration method presented here is the same to the one used in [1].

The received baseband signal is sampled at a high enough sampling rate (1/ T_s). The time interval $\left[(k-1)T_s,(k+1)T_s\right]$ is determined where $t = kT_s$ corresponds to the maximum of the correlation function. The two maximum values are selected from the samples at $\{(k-1)T_s, kT_s, (k+1)T_s\}$. Next, the procedure of halving is performed between the two selected sampling instants. The value of the correlation function is then evaluated for the new mid point by interpolation process and then the maximum two is selected among the three values of the samples. The iterative algorithm is shown in Figure 4.5.

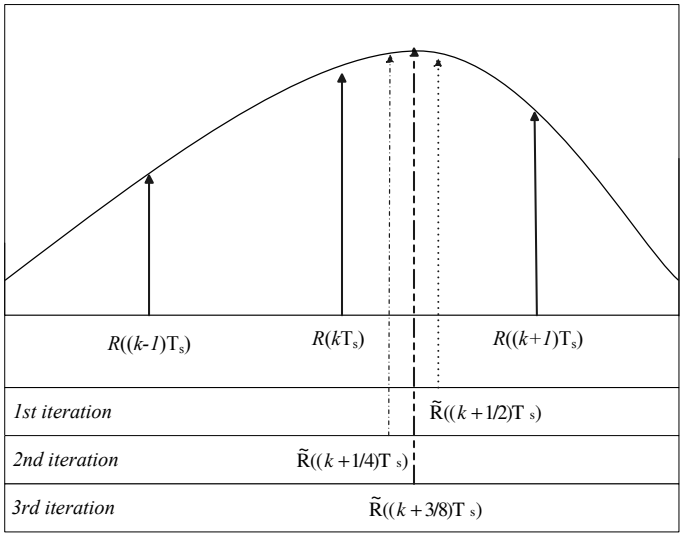

Figure 4.5. Illustration of the iteration process.

The processes of "interpolation & calculation" of the correlation function and "maximum value selection" are then repeated until a sufficient number of iterations.

4.3.3. Interpolation

As stated in 3.2.1 before, interpolation in receivers is generally employed to shift the received signal in time by the estimated timing offset value. In this section, the interpolation is used for approximating the correlation function for the times other than the sampling instants.

The ideal interpolation formula, which forms the basis of sampling theorem is, [30],

$$\tilde{R}(t) = \sum_{-\infty}^{\infty} R(mT_s) \frac{\sin\left(\frac{\pi}{T_s}(t - mT_s)\right)}{\frac{\pi}{T_s}(t - mT_s)}, \tag{4.18}$$

where T_s is the sampling period. The tilde indicates that the correlation function has been produced using interpolation.

If the signal is sampled at a rate higher than the Nyquist rate, various other recovery filters can be designed.

In this thesis, the raised cosine filter is used as the interpolation filter. The impulse response of the raised cosine filter can be written as

$$h_l(t) = \sin c(2B_T t) \frac{\cos(2\pi\rho B_T t)}{1 - 16\rho^2 B_T t^2}, \tag{4.19}$$

where B_T is the symmetry frequency and ρ is the roll-off factor. Figure 4.6 shows the impulse response of the raised cosine filter for different values of ρ with $B_T = 1/2T$.

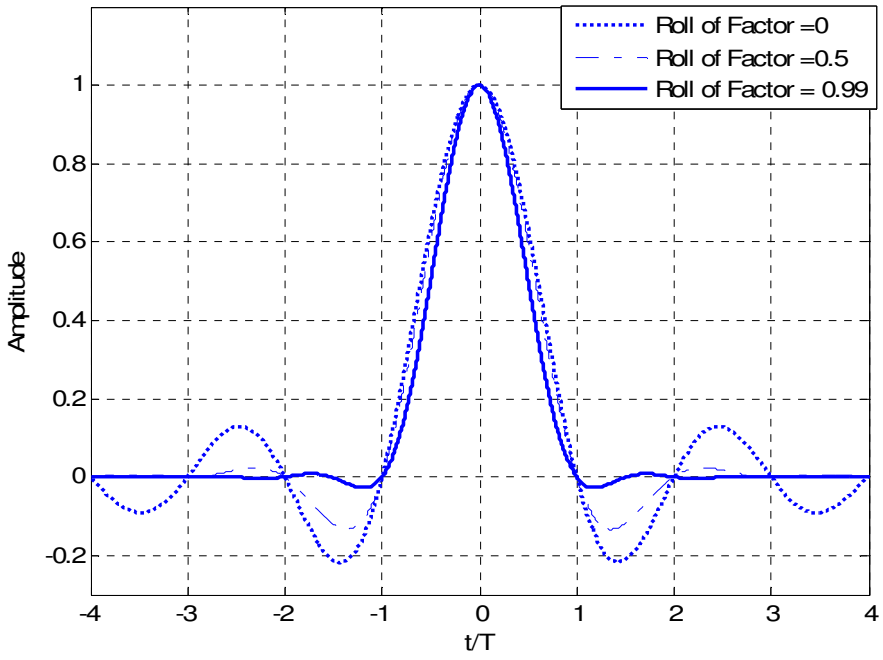

Figure 4.6 Impulse response of raised cosine filter.

According to the illustration of the samples in Figure 4.7, with an oversampling rate of $N = T/T_s$, the timing instants can be defined as

$$t_k = kT_s + \hat{\tau} \tag{4.20}$$

where $\hat{\tau}$ is the fractional delay and k is the index of the nearest sampling instant.

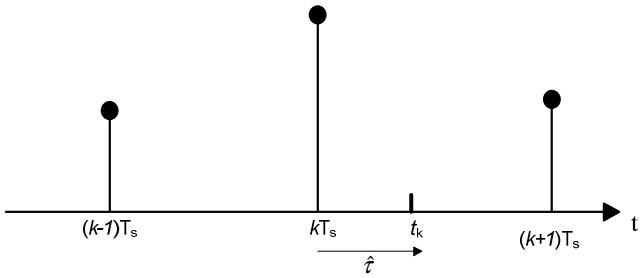

Figure 4.7 Illustration of k and $\hat{\tau}$ in determining the timing instant.

Using the notation in (4.20) the interpolation formula becomes

$$\tilde{R}(t_k) = \sum_{m=k-L_2}^{k+L_1} R(mT_s) h_l\left[(k-m)T_s + \tau\right], \tag{4.21}$$

with $h_l(t)$ given in (4.19) with $B_T = 1/2T_s$. The summation in (4.21) is truncated to a smaller length $N_l = L_1 + L_2 + 1$. By changing the summation index in (4.21) we may obtain

$$\tilde{R}(t_k) = \sum_{i=-L_1}^{L_2} R\left[(k-i)T_s\right] h_l(iT_s + \tau), \tag{4.22}$$

The length of the interpolator, $N_l = L_1 + L_2 + 1$, used in simulations has been chosen to ensure that the variance of the timing estimates is tolerable.

4.3.4. Discussion on the Parameters

In this subsection the parameters which affect the performance of the proposed timing recovery scheme [1] for GMSK signals are discussed. For simplicity, discussion on the parameters is based on simulations with AWGN channel. The proposed timing recovery scheme with fading channel application will derive benefit from the result of this section.

Sampling rate and number of iteration:

Sampling rate can be given by $T_s = \frac{T}{N}$ where N is a positive integer. N=4 is generally a good choice [1] Sensitivity of the timing epoch from the proposed timing recovery scheme depends on sampling rate and number of iteration may be expressed as $\frac{1}{N * 2^{n_i+1}}$. Note that increasing the sampling rate will decrease the number of iteration. With N=4 and n_i=4, this results in a sensitivity of $\frac{1}{128}$ of a symbol period.

Observation interval:

The final accuracy is limited by the variance of the timing estimate. The primary factor in obtaining a low variance of the timing estimate is the length of the observation interval. The observation interval refers to the block length L_0 used in the correlation which can be defined as the number of the symbols used in timing recovery, i.e., $T_0 = L_0 T$. Figure 4.8 gives the relation of the variance to the block length for different SNR. As is seen, the block length of 32 symbols is a good choice even for low SNR values. Considering the moderate SNR values timing recovery can also be performed satisfactorily for smaller L_0 values.

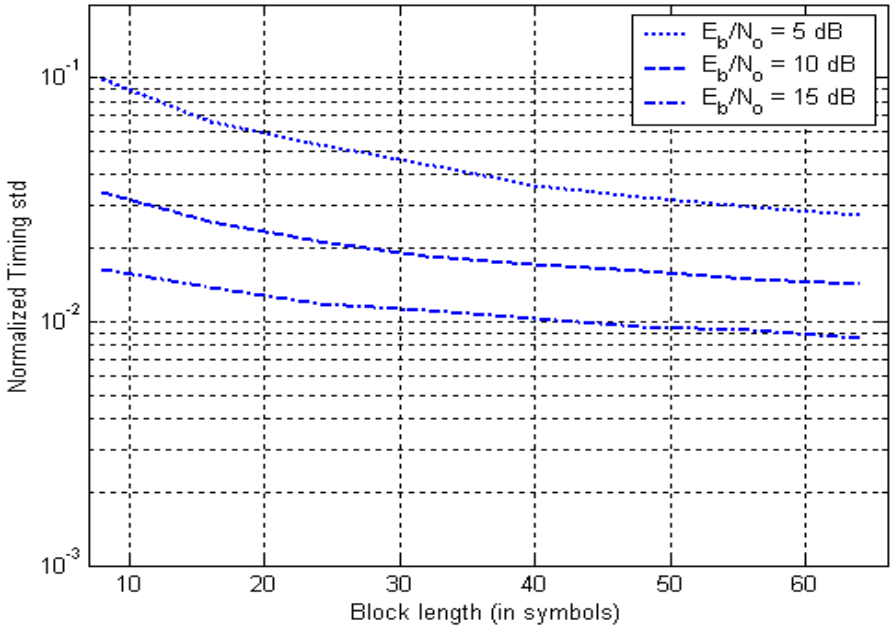

Figure 4.8 Normalized timing standard deviation for different SNR values.

Interpolation length :

In this subsection interpolation length affects on the variance of the timing estimate is discussed.

Useful information about the timing epoch is in the main interval which contains the peak value at the matched filter output. Figure 4.9 shows a typical matched filter output. The components used in the interpolation should contain almost all the necessary samples; however, as the interval exceeds the useful part, timing errors may result.

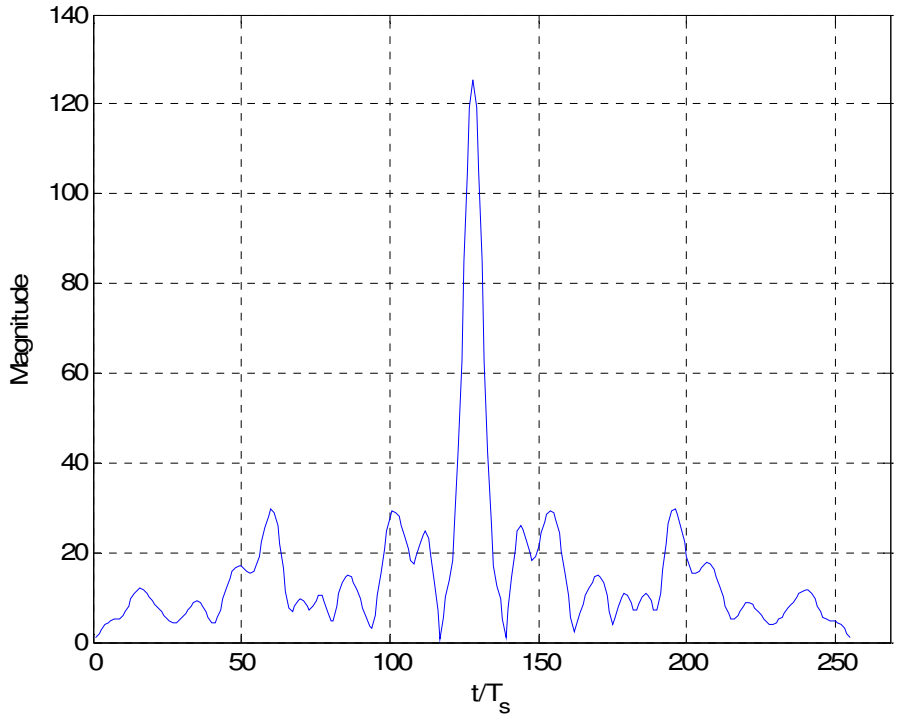

Figure 4.9 Matched filter output with $L_0 = 32$, SNR = 30 dB.

Normalized standard deviation of the timing values are calculated for different length of observation length and interpolation length and Table 4.1 is formed.

As discussed in [1] for MSK, there is a remarkable decrease when interpolation length is increased from 3 to 5 for GMSK, and the results for the interpolation lengths of 5 and 7 do not differ much. For simplicity interpolation length of 5 will be preferred in the simulations in Chapter 5.

Table 4.1 Normalized timing standard deviation for different interpolation length and observation interval.

	$L_0 = 8$			$L_0 = 16$			$L_0 = 32$		
SNR	$N_i = 3$	$N_i = 5$	$N_i = 7$	$N_i = 3$	$N_i = 5$	$N_i = 7$	$N_i = 3$	$N_i = 5$	$N_i = 7$
0 dB	0.4348	0.4301	0.4303	0.2116	0.1989	0.1977	0.1371	0.1059	0.1042
10dB	0.1259	0.0330	0.0339	0.1250	0.0242	0.0256	0.1250	0.0184	0.0198
20dB	0.1257	0.0060	0.0118	0.1250	0.0085	0.0087	0.1250	0.0065	0.0067

Interpolation filter roll-of factor:

The symmetry frequency of the interpolation filter is taken as $1/T_s$. Considering the bandwidth of the GMSK signal interpolation filter with the roll-off factor of 0.5, 0.6 and 0.7 may be used. The variances of the timing estimate with different roll-off factor are discussed. Table 4.2 gives the normalized standard deviation of the timing values for interpolation filter with roll of factor of 0.5, 0.6 and 0.7.

Table 4.2 Normalized timing standard deviation for $L_0 = 32$, $N_i = 5$.

SNR	Roll-of Factor		
	ρ =0.5	ρ =0.6	ρ =0.7
0 dB	0.1165	0.1045	0.10294
10dB	0.0102	0.0187	0.0232
20dB	0.0017	0.0065	0.0080

Smaller values of the roll-of factor result in smaller variance, except for very low SNR operation. Roll of factor affect will be also discussed for frequency-selective fading channel application in the next chapter.

CHAPTER 5

SIMULATION AND RESULTS

5.1 INTRODUCTION

The proposed decision-directed symbol synchronizer model has been developed in MATLAB. Although MATLAB is based on discrete time signals, the continuous-time signals are represented by their discrete samples taken at a rate much greater than the Nyquist rate for a proper simulation.

In this chapter, firstly the model of the simulated system is presented. Next, several properties of the GMSK modulated signal, the channel model and channel tap generation process and methods of construction on the matched filter are discussed. Performance of the symbol synchronizer in AWGN channel is compared with MCRB for different observation intervals. Finally, the tracking performance of the synchronizer is compared with Mazo criterion.

5.2 SIMULATION MODEL OF THE COMMUNICATION SYSTEM

The signal processing in the simulations is realized in baseband. The general simulated diagram is shown in Figure 5.1.

When the observation interval is selected as 16, the training sequence is chosen from one of the special training sequence codes from Table 2.1. In other situations, the training sequence is generated randomly. Information bits are generated randomly. The training sequence and information sequence are assembled as training sequence is placed in front of the data burst. The data burst is encoded and then modulated with GMSK modulator. In the simulation, linear approximated GMSK is used and features of the GMSK modulated signal are presented in 5.2.1.

Then the GMSK modulated samples are passed through the multipath fading channel. Details related to the simulated multipath fading channel are presented in 5.2.2. White Gaussian noise is also added to the channel output.

At the receiver part, the received signal is passed through a low-pass filter (LPF) to reject the out of band components. An 8-pole Butterworth filter is used as the LPF $g_R(t)$ in the simulations.

In the synchronizer, firstly the initial timing is realized by acquisition mode of the synchronizer which uses the training sequence. And then timing knowledge is extracted by tracking mode of the synchronizer which uses the tentative decisions from MLSE receiver (Viterbi Algorithm). Error free tentative decisions from Viterbi algorithm are assumed. In each observation interval, symbol synchronizer makes use of extracted timing knowledge in former observation interval.

Performance of the proposed symbol synchronizer for GMSK modulated signal depends on the matched filter structure. Several methods used on the design of the matched filter structure are presented in 5.2.3.

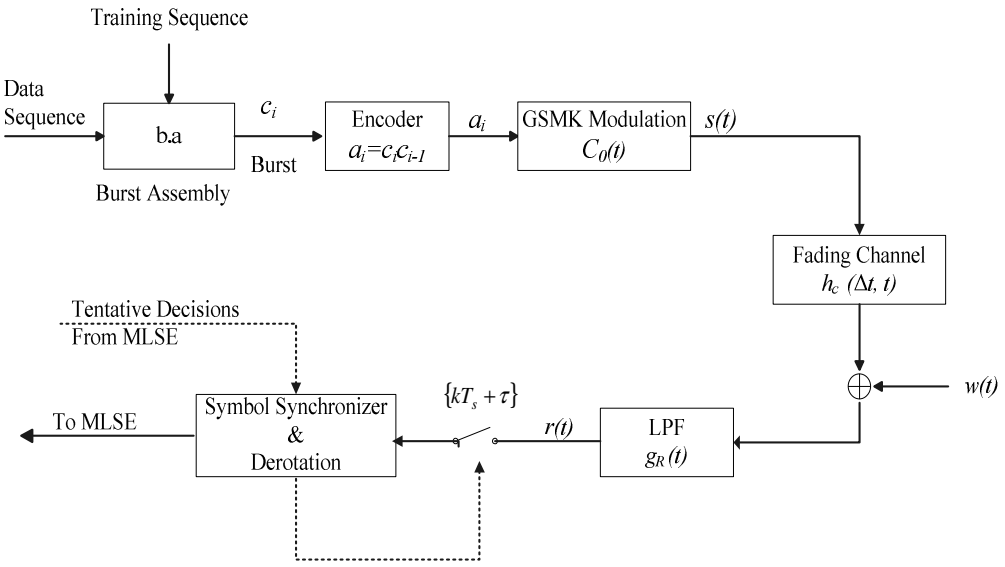

Figure 5.1 General block diagram of the simulated system.

5.2.1 GMSK Modulated Signal

Linear approximation of the GMSK signal in equation (2.27) is used in the simulations. Features of the simulated GMSK signal with BT of 0.3 are tested in order to make sure validity of the modulated signal.

As expected in 2.3.1, complex envelope of the approximated signal is not constant. Figure 5.2 depicts the envelope of the linear approximated GMSK signal. For BT $\rightarrow \infty$ GMSK signal converges to MSK signal and envelope of the GMSK signal will be constant.

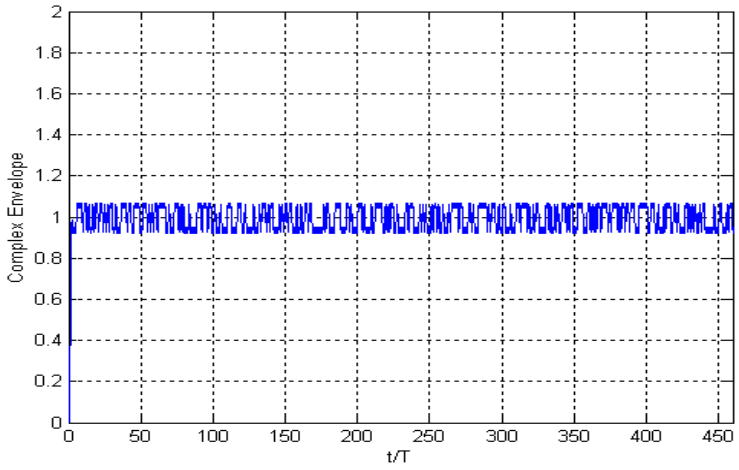

Figure 5.2 Complex envelope of the approximated GMSK signal.

The other feature of the approximated linear GMSK signal is its power spectrum density. The similarity between the curves shown in Figure 5.3 is convinced about validity of the simulated GMSK signal.

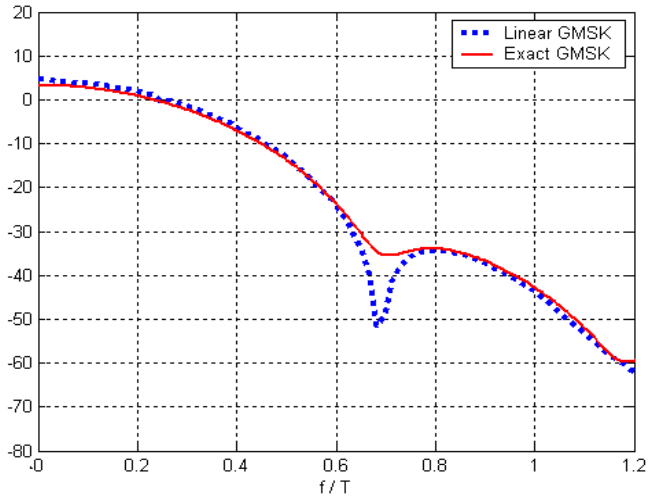

Figure 5.3 Power spectrum density of linear GMSK and exact GMSK signal.

5.2.2 Simulated Channel Specifications

In the simulation model, tapped delay line (TDL) model of the time variant frequency selective fading channel is used. Channel model is shown in Figure 5.4.

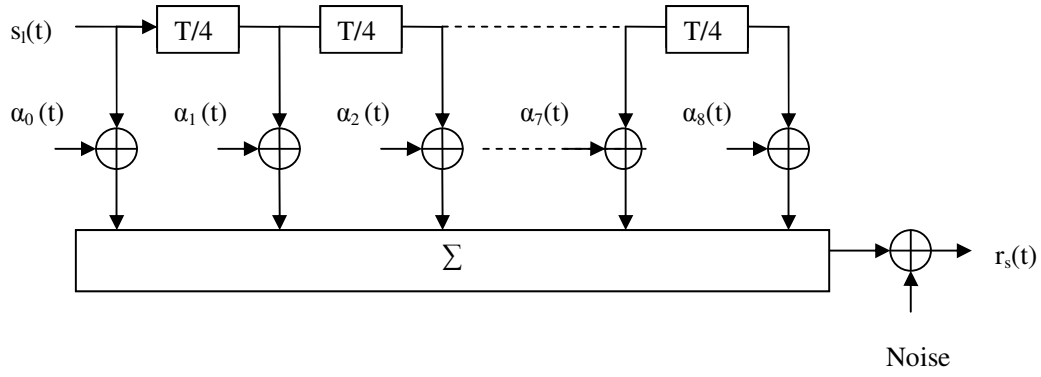

Figure 5.4 Tapped delay line model of the multipath fading channel.

Equivalent low-pass channel is expressed by the time-variant impulse response

$$h_c(\Delta t;t) = \sum_n \alpha_n(t)\delta(\Delta t - \Delta t_n) \tag{5.1}$$

where Δt is the time delay between the successive taps of the TDL model of the channel. Generally $\Delta t \leq 1/B$ is satisfied, where B is the two sided bandwidth of the GMSK signal. In simulations Δt is chosen as $\Delta t = T_s = T/4$. Time spread of the channel is taken as 2T, so that nine taps exist in the simulated channel.

Taps are adjusted as explained in section 2.2.3. As a brief summary, a complex Gaussian signal is generated by the independent complex white Gaussian generator. This signal is shaped by a filter denoted by *H(f)* has a normalized power of 1. The bandwidth of the tap-gain function is determined the maximum Doppler

frequency. Bit rate used in GMSK is 270.83 kHz, due to $T_s = \frac{T}{4}$, the sampling rate of the signal is 1080 kHz but according to our scenario the shaping filter bandwidth is narrower than 150 Hz. Therefore, to increase the accuracy the tap generation function is sampled at a much lower rate than the sampling rate of the system, and then an interpolating filter is used to obtain actual the sampling rate. The sampling rate of the tap generation block is selected as 10.8 kHz. The resulting sampling rate of the tap generation process is expanded by a factor of 100. The interpolation is realized by a Raised-cosine interpolation filter with roll-of factor of 0.9. The interpolation filter output is scaled with the standard deviation calculated from equation 2.9 for each independent taps. As summary, tap generation procedure is shown in Figure 5.5.

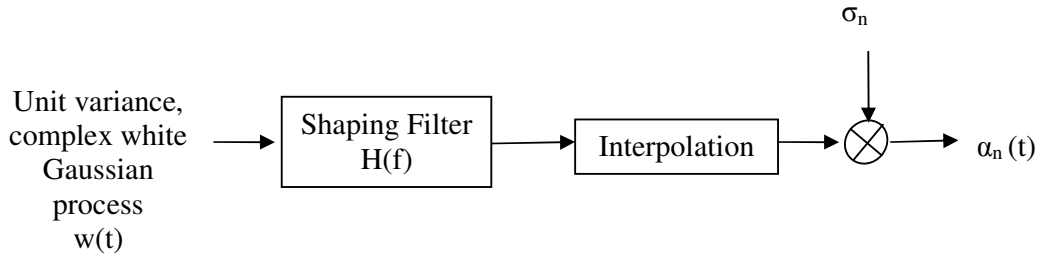

Figure 5.5 Generation of taps.

In the simulations two scenarios are used. Both of them have power delay profile for urban (non-hilly) area (TU) channel shown in 2.2.2.2. In the first scenario, a vehicle traveling at a speed of 50km/h is assumed and carrier frequency is 900 MHz, whereas in the second scenario vehicle is faster, 90km/h and its carrier frequency is 1800 MHz. First one generates f_d =42 Hz (v=50 km/h and f_c= 900MHz) and the other one generates f_d =150 Hz (v=90 km/h and f_c= 1800MHz).

5.2.3 Methods on the Matched Filter

The conclusive aim of a symbol synchronizer is to estimate the most likely value of the timing epoch. In section 4.3.1 the correlation (matched filter) method was discussed. The estimation of timing epoch is obtained by received signal passed through the filter, which is matched to the reference signal over the observation interval (L_0). This section presents two methods, called "Method A" and "Method B", on construction of the matched filter in other words the reference signal.

As explained in 4.3.1, in the acquisition mode a GMSK modulated signal with the training sequence known by the receiver is used and in the tracking mode a GMSK modulated signal with the tentative decisions, coming from MLSE receiver is used. For the GMSK signal with BT=0.3, pulse shaping function *g(t)* in Figure 2.8 spans a time interval of approximately 4 symbol durations. Due to this, for the each observation interval the GMSK modulated signal spans a time interval of 3 symbol durations through the next observation interval. The last 3 symbol durations of the modulated signal is called as "tail". For each observation interval GMSK modulated signal denotes as $s_i(t)$. Beginning and ending points of the $s_i(t)$'s are shown in Figure 5.6.

Method A constructs the reference signal by adding the first interval of L_0 symbol duration of the GMSK modulated signal of the currently observation interval and last interval of 3 symbol duration of GMSK modulated signal from the previous observation interval. Figure 5.7 depicts construction of the reference signal, $r_i(t)$ by Method A.

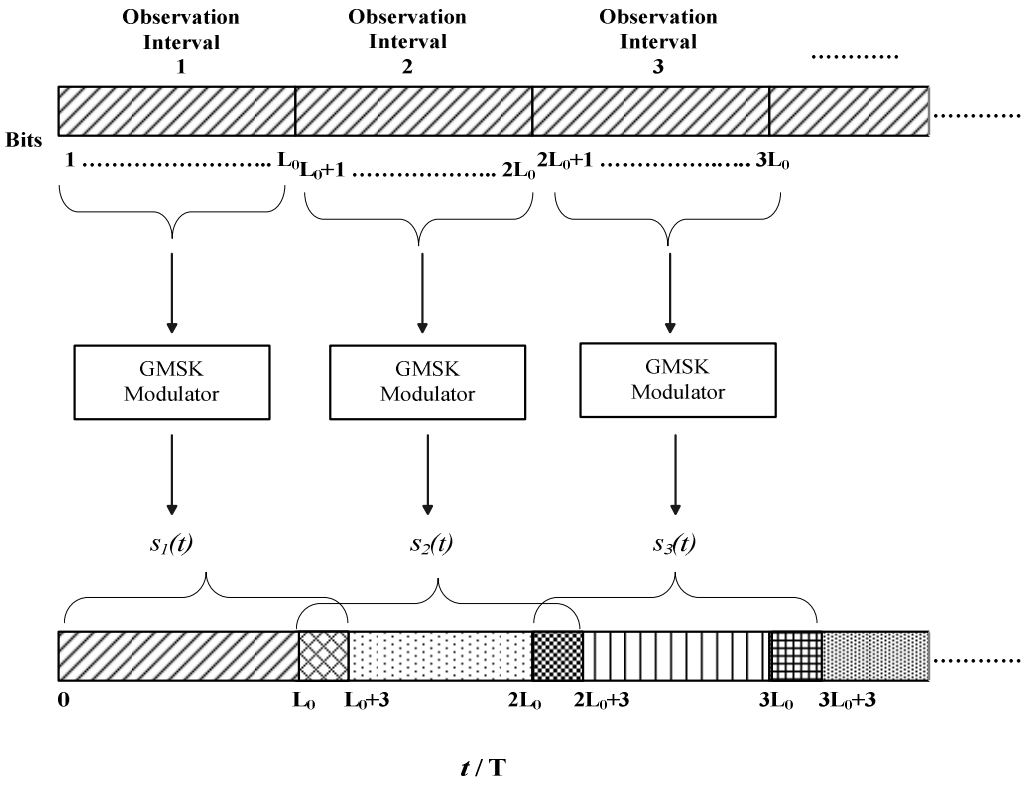

Figure 5.6 Location of $s_i(t)$.

In Method B, the reference signal is ISI free part of the GMSK modulated signal with tentative decisions from MLSE. Method A does not take into account the channel ISI arising from multipath fading channel. Method B assumes that the channel delay has maximum 2 symbol durations. First 5 symbol duration part of the GMSK modulated signal is called "dirty" due to modulation and channel delay spread. Method B constructs the reference signal $r_i(t)$ by extracting the *dirty* and *tail* parts from $s_i(t)$. So reference signal according to the Method B is not affected from the previous data block. Figure 5.8 depicts construction of the reference signal $r_i(t)$ according to Method B.

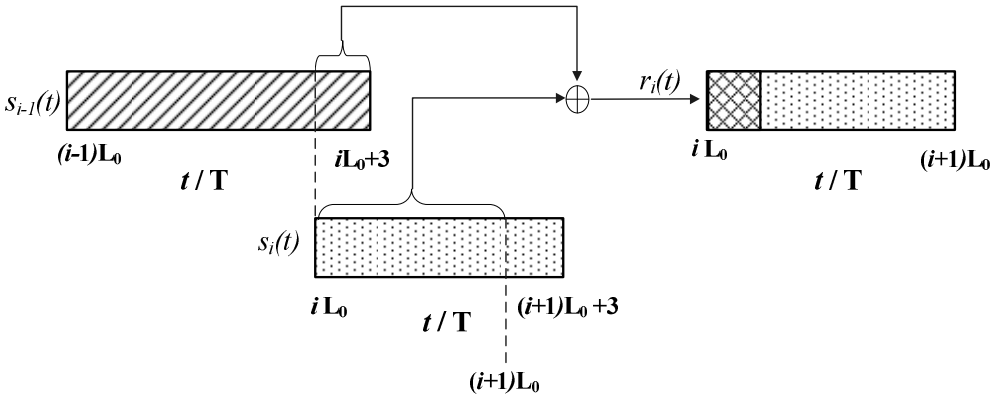

Figure 5.7 Construction of the reference signal by Method A.

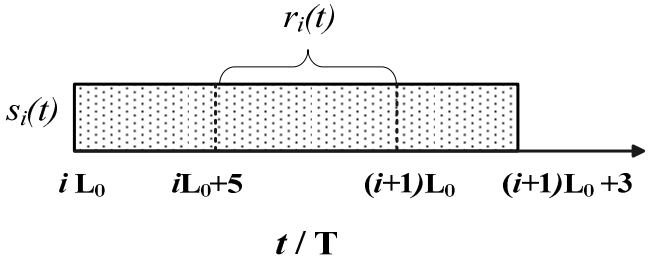

Figure 5.8 Construction of the reference signal by Method B.

Comparisons of Methods A and B are obtained by simulations. Figure 5.9 – Figure 5.12 show the results pertaining to timing estimates using Method A and B. under the effects of the multipath fading channels. The performance is given for block length of L_o = 16 or L_o = 32. In order to illustrate effect of the fast variations, two channel scenarios are used as explained before. Interpolation is performed within an interval of N_i = 5, and roll-off factor of 0.6.

As seen from the figures the curves are very close to distinguish the differences thus an rms error is calculated for each situation. The rms error is defined as;

$$E = \sqrt{\frac{1}{M}\sum_{k=1}^{M} e(k)^2}\ , \tag{5.2}$$

where *e(k)* is the difference between the normalized timing phase by Mazo criterion and the normalized timing estimation from the synchronizer for each sampling interval, M is the total number of sampling interval. In the simulations rms error values are given in order to discuss performance with Method A and B for each curve.

In Figure 5.9 and Figure 5.10, the same channel in the first scenario is simulated for the block length of L_o = 16 and 32 respectively. As can be seen from Figures 5.9, 5.10; the timing curves are very close to each other and to that predicted by using the Mazo criterion.

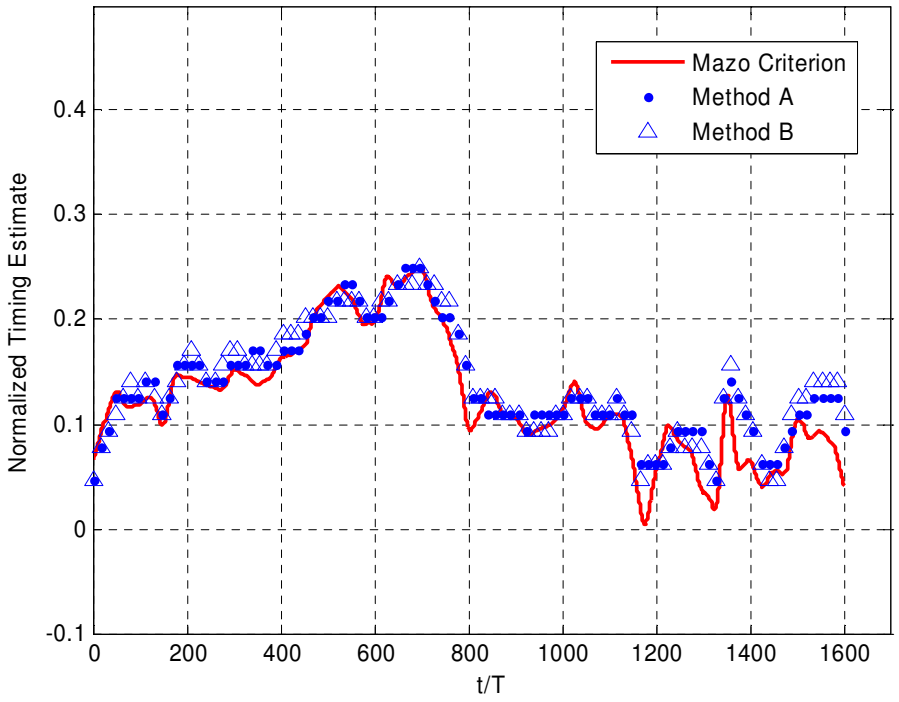

Figure 5.9 Comparison of the Methods A and B
(L_o =16 , SNR=30dB, v=50 km/h and f_c= 900MHz).

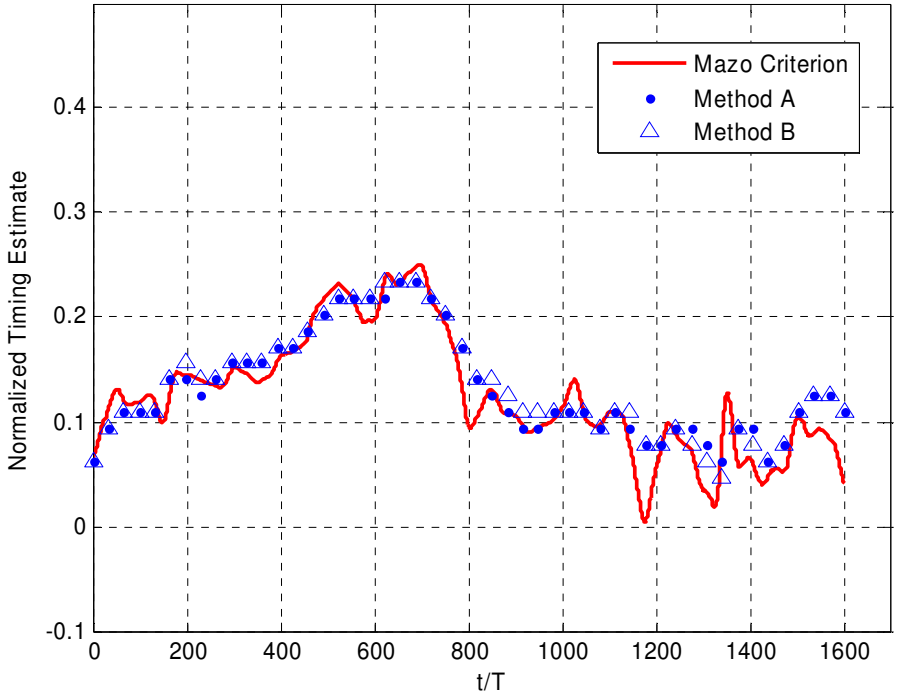

Figure 5.10 Comparison of the Methods A and B
(L_o =32 , SNR=30dB, v=50 km/h and f_c= 900MHz).

In order to compare performance using Method A and B simulations in Figures 5.9 - 5.10, Table 5.1 is formed.

Table 5.1 The rms error values for the simulations in Figure 5.9 and 5.10.

Channel: v=50 km/h and f_c = 900MHz		**rms error**
Method A	L_o =16	0.0570
Method B	L_o =16	0.0571
Method A	L_o =32	0.0627
Method B	L_o =32	0.0618

The rms error values for Method A and B are nearly the same for the block length of L_o = 16 but Method B gives a better performance for the block length of L_o = 32 than Method A.

As another case, a much faster channel in the second scenario is used. Normalized timing estimation of the synchronizer with using Method A and B are illustrated in Figures 5.11-5.12 for the block length of L_o = 16 and 32 respectively. The rms error values are calculated and given in Table 5.2.

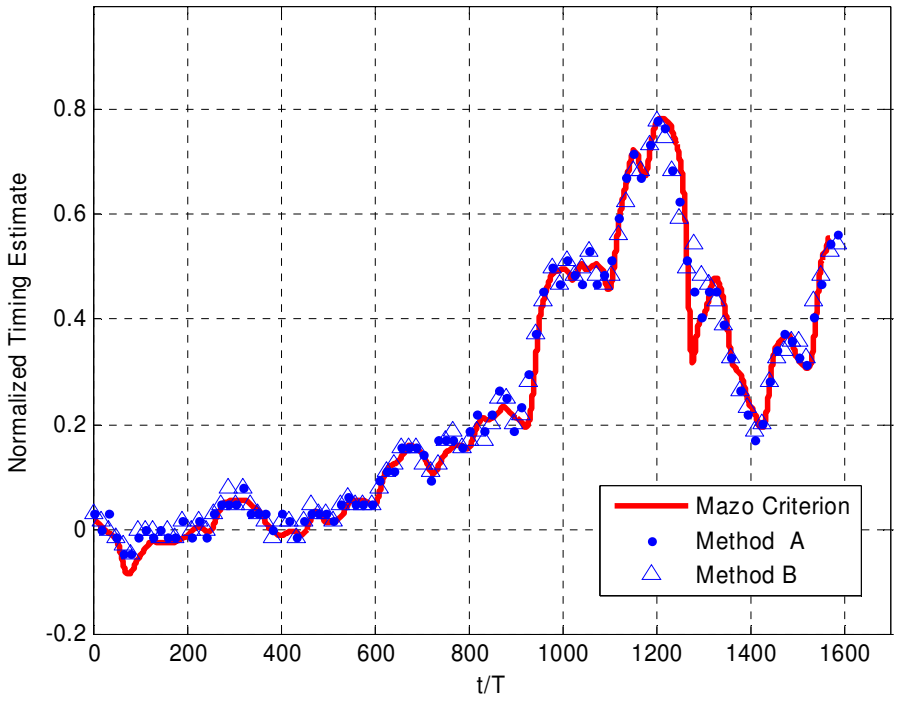

Figure 5.11 Comparison of the Methods A and B
(L_o =16 , SNR=30dB, v=90 km/h and f_c= 1800MHz).

Table 5.2 The rms error values for the simulations in Figure 5.11 and 5.12.

Channel: v=90 km/h and and f_c = 1800MHz		**rms error**
Method A	L_o =16	0.1249
Method B	L_o =16	0.1236
Method A	L_o =32	0.1291
Method B	L_o =32	0.1278

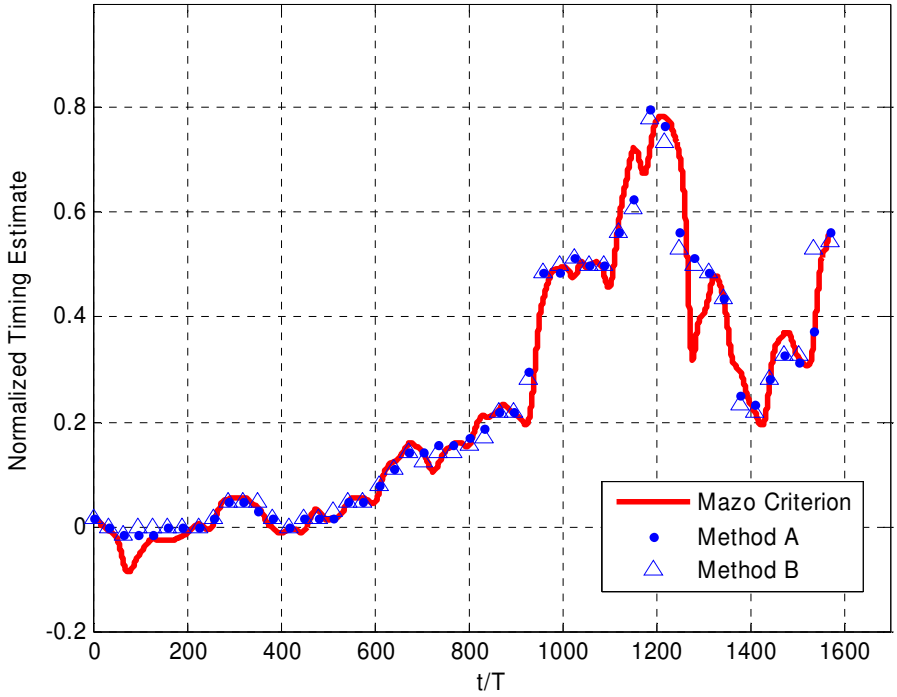

Figure 5.12 Comparison of the Methods A and B
(L_o =32 , SNR=30dB, v=90 km/h and f_c= 1800MHz).

Tracking abilities of the synchronizer with using Methods A and B are almost the same except that slight increase in the rms error with Method A for L_o =16, rms error difference becomes larger for L_o =32.

As a summary, to achieve timing recovery in GMSK signals the matched filter used in the correlation method must be improved due to different pulse shape of GMSK. Therefore two methods are developed and performance of the synchronizer with using the methods is discussed. According to the simulation results, it is assessed that Method B has a slightly better performance under fast fading channel So Method B is used for the simulation in the next section.

5.3 TRACKING PERFORMANCE OF THE PROPOSED SYMBOL SYNCHRONIZER

In this section performance of the proposed synchronizer is tested. The Modified Cramer Rao bound and Mazo criterio are used in order to compare the performance of the synchronizer in additive White Gaussian and multipath fading channels, respectively, as explained in 4.2.

5.3.1 Performance on the AWGN Channel

The performance of the proposed synchronizer is tested in additive white Gaussian channel. In Figures 5.13 and 5.14, the standard deviation of the timing estimate is compared with the MCRB for two different block lengths.

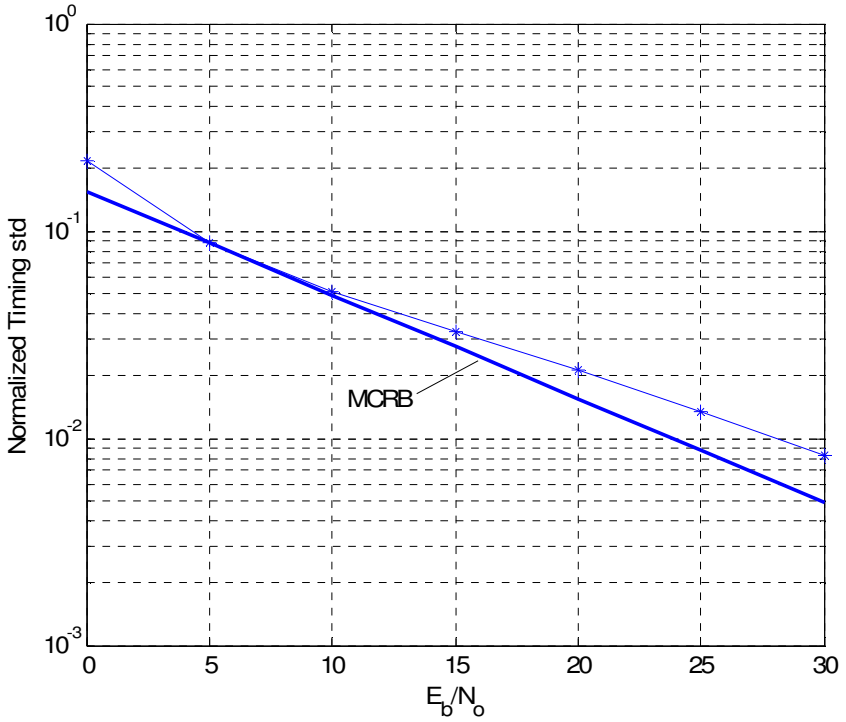

Figure 5. 13 Performance of the symbol synchronizer for L_o=16.

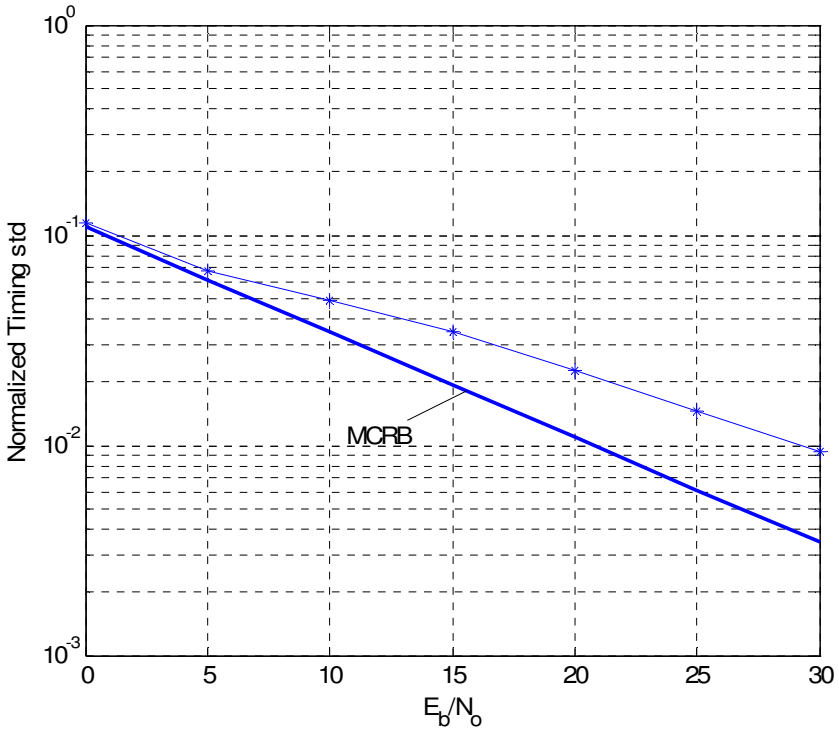

Figure 5.14 Performance of the symbol synchronizer for L_o=32.

The simulations in this subsection are implemented in order to observe performance under AWGN channel. As expected improvement with increasing the block length from 16 to 32 is obtained. Because MCRB is not the true bound so that deviations for both cases are considerable.

5.3.2 Performance on the Frequency Selective Fading Channel

In this section the effects of the multipath fading channel on timing extraction are discussed. The initial recovery of the timing epoch is performed using a training sequence with a specified block length. Then tracking of the channel is performed based on matched filter method using Method B. For comparison, the performance is

given for different values of the parameters; observation interval, SNR and roll of factor of the interpolation filter.

Firstly, the tracking performance of the proposed timing recovery scheme is tested for the first channel condition at 30 dB SNR for the block length of L_o = 16, 32 and 64. Figure 5.15 shows the tracking ability for the performance for the block length of L_o =16 and 32. Simulation results are very similar to that obtained from the Mazo criterion. Figure 5.16 depicts a comparison of the performances for block lengths of L_o =16 and 64. As seen from the figure, the synchronizer for the one with block length of L_o =64 can not track the channel variations as well as for the block length of L_o =16. The rms error values for the simulations in Figure 5.15 and 5.16 are given in Table 5.3.

Table 5.3 The rms error values for the simulations in Figure 5.15 and 5.16.

Channel: v=50 km/h and f_c = 900MHz, SNR=30dB, ρ = 0.6, Method B	
Block Length (L_o)	**RMS Error**
L_o =16	0.0571
L_o =32	0.0618
L_o =64	0.0688

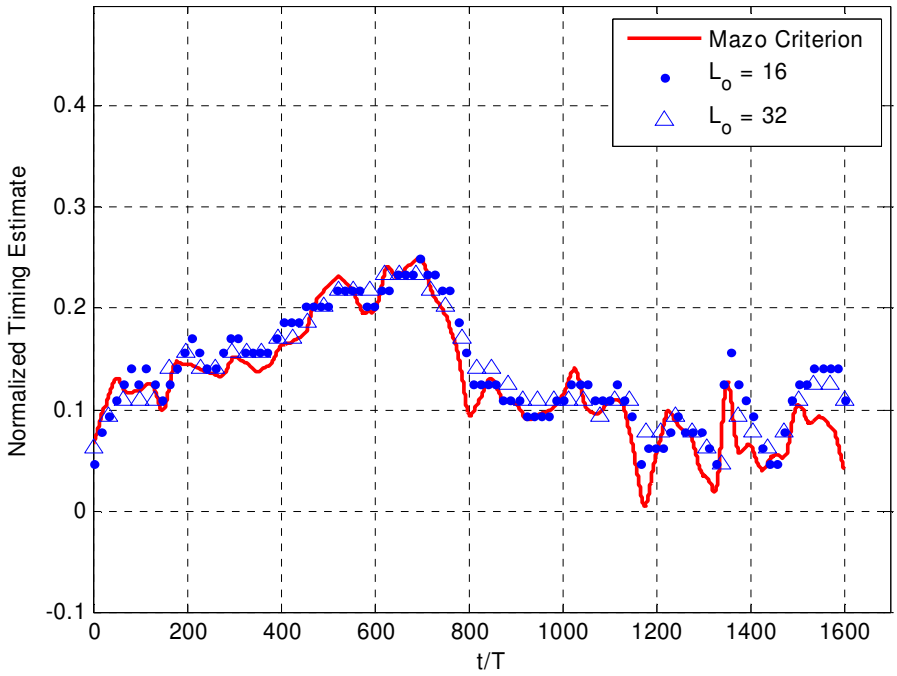

Figure 5.15 Tracking performance of the proposed synchronizer for two observation intervals (SNR=30dB, v=50 km/h and f_c= 900MHz).

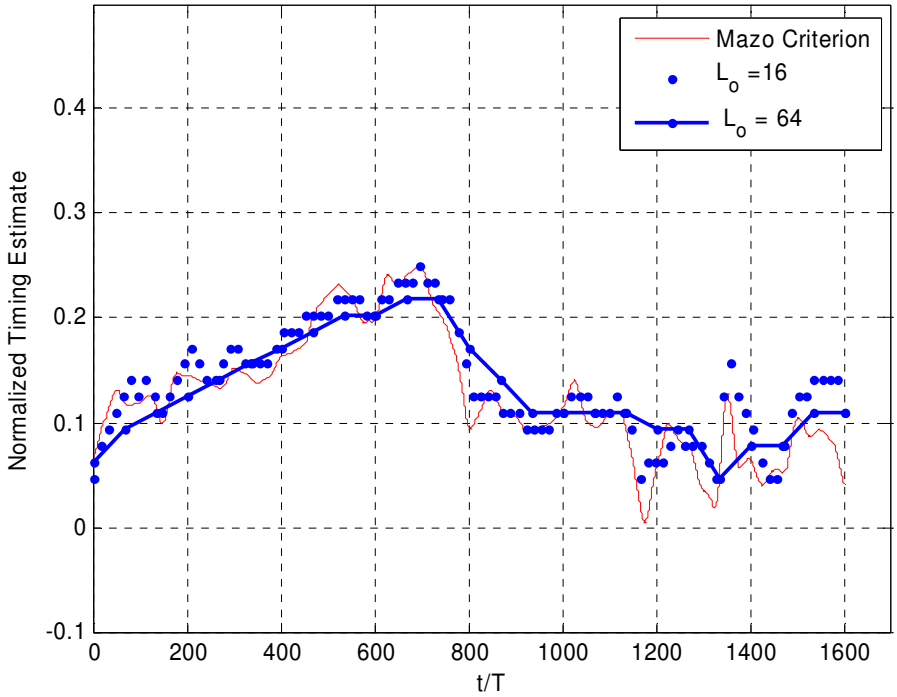

Figure 5.16 Tracking performance of the proposed synchronizer for two observation intervals (SNR=30dB, v=50 km/h and f_c= 900MHz).

The tracking performance of the proposed timing recovery scheme is tested for the first channel condition at 30 dB SNR, for the block length of L_o=32 for different roll of factor of the interpolation filter. Figure 5.17 shows the tracking ability for the performance for 0.5, 0.6 and 0.7 roll of factor of the interpolation filter. The rms error values for the simulations in Figure 5.17 are given in Table 5.4.

Table 5.4 The rms error values for the simulations in Figure 5.17.

Channel: v=50 km/h and f_c = 900MHz, L_o =32, Method B	
Roll of Factor (ρ)	**rms error**
0.5	0.0696
0.6	0.0618
0.7	0.0643

Figure 5.18 shows the tracking performance of the proposed timing recovery scheme is tested for the first channel condition for block length of L_o=32 at 10 dB, 20 dB and 30 dB SNR. The rms error values for the simulations in Figure 5.18 are given in Table 5.5.As expected, rms error for higher SNR is smaller.

Table 5.5 The rms error values for the simulations in Figure 5.18.

Channel: v=50 km/h and f_c = 900MHz, L_o =32, ρ =0.6, Method B	
SNR	**rms error**
10dB	0.0661
20dB	0.0640
30dB	0.0618

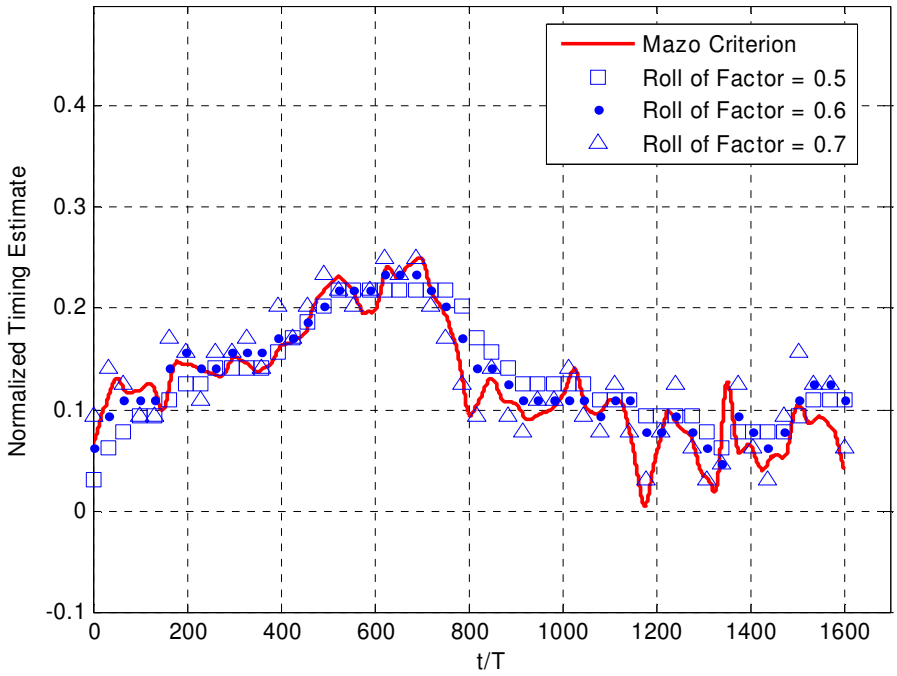

Figure 5.17 Tracking performance of the proposed synchronizer for different roll of factor values. (L_o =32, SNR=30dB, v=50 km/h and f_c= 900MHz).

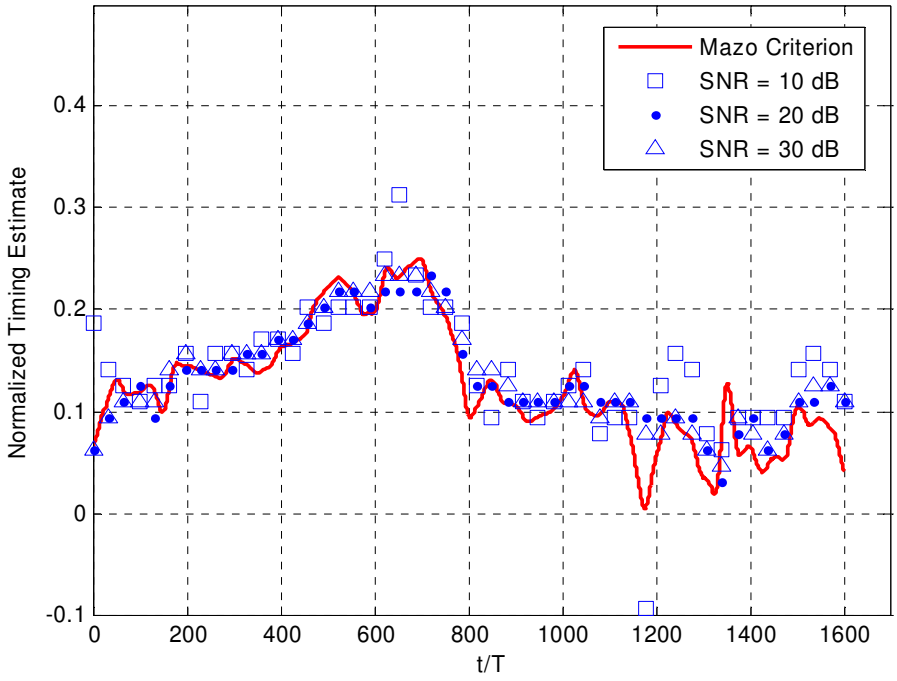

Figure 5.18 Tracking performance of the proposed synchronizer for different SNR values. (L_o =32, v=50 km/h and f_c= 900MHz).

The simulations for the first channel are repeated for a faster channel in the second scenario. The tracking performance of the proposed timing recovery scheme is tested at 30 dB SNR for block length of L_o=8, 16, 32 and 64. Figure 5.19 shows the tracking ability for block lengths of L_o=16 and 32. Simulation results are very similar to the values obtained from the Mazo criterion. Figure 5.20 depicts a comparison of the performances for block lengths of L_o=16 and 64. Figure 5.20 clearly shows the insufficiency of the synchronizer for block length of L_o=64 can not track the channel variations whereas the synchronizer for the block length of L_o = 16 can track the channel variation successfully.

The rms error values for the simulations in Figure 5.19 and 5.20 are given in Table 5.6. As expected, the rms error values are worse than error figures of the first channel. Table 5.6 shows the block length of L_o = 8 and L_o = 64 are not good candidates. Timing estimate of the synchronizer for the block length of L_o=64 is too sparsely updated that it can not track the channel variations. For the synchronizer using a block length of L_o=8, observation interval is too short to provide sufficient noise suppression.

Table 5.6 The rms error values for the simulations in Figure 5.19 and 5.20.

Channel: *v*=90 km/h and f_c = 1800MHz, SNR=30dB, ρ=0.6, Method B	
L_o	**rms error**
L_o=8	0.1414
L_o=16	0.1236
L_o=32	0.1278
L_o=64	0.1421

As a result of Table 5.3 and 5.6, observation interval L_o=16 and L_o=32 are selectable.

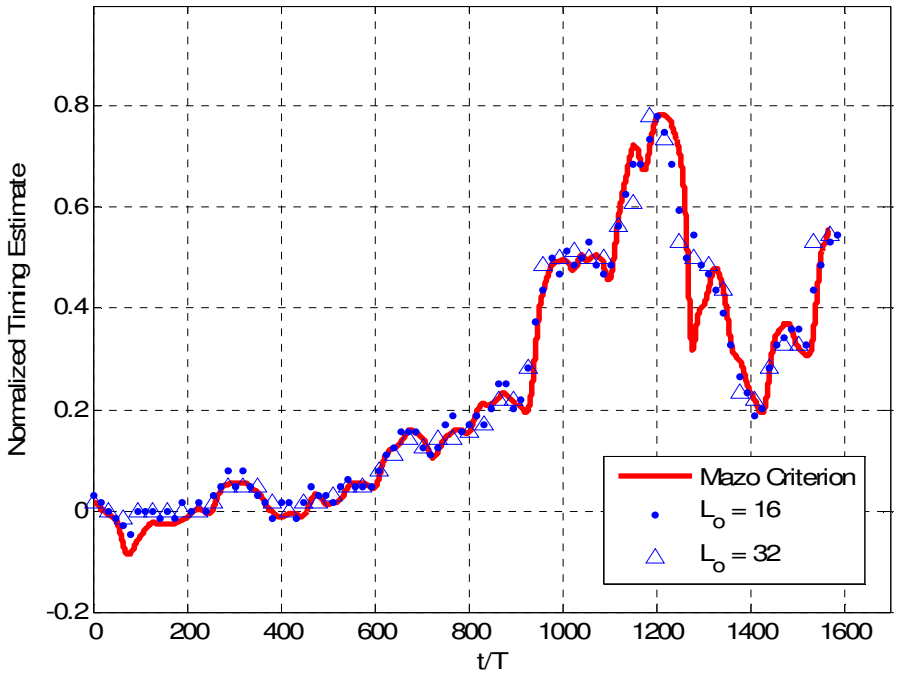

Figure 5.19 Tracking performance of the proposed synchronizer for two observation intervals (SNR=30dB, v=90 km/h and f_c= 1800MHz).

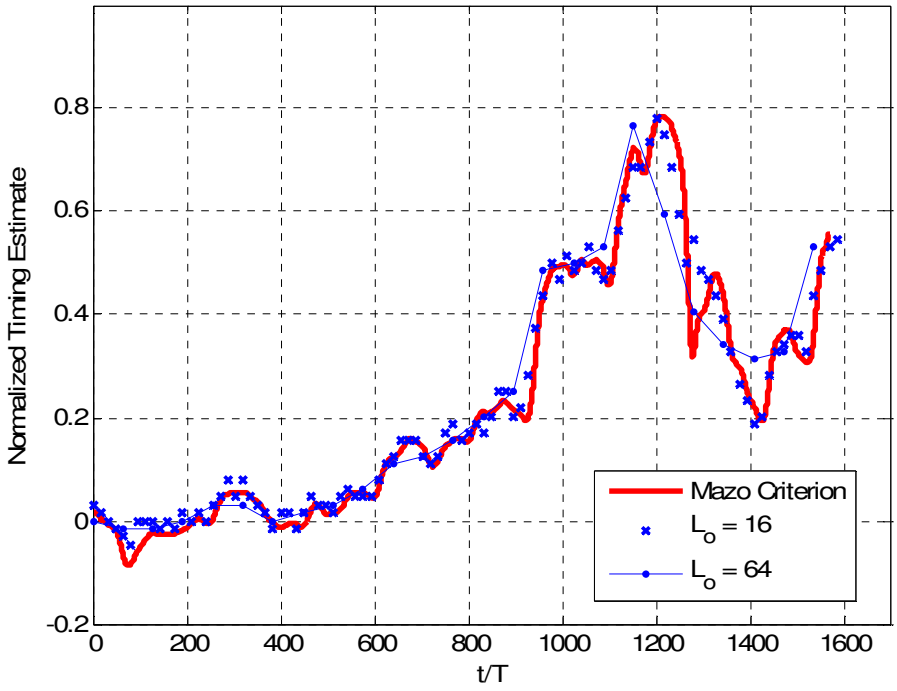

Figure 5.20 Tracking performance of the proposed synchronizer for two observation intervals (SNR=30dB, v=90 km/h and f_c= 1800MHz).

The tracking performance of the proposed timing recovery scheme is tested for the second channel condition at 30 dB SNR, for the block length of L_o=32 and a different roll of factor of the interpolation filter. Figure 5.21 shows the tracking ability for the performance for 0.5, 0.6 and 0.7 roll of factor of the interpolation filter. The rms error values for the simulations in Figure 5.21 are given in Table 5.7.

Table 5.7 The rms error values for the simulations in Figure 5.21.

Channel: *v*=90 km/h and f_c = 1800MHz, L_o =32, SNR=30dB, Method B	
Roll of Factor	**rms error**
0.5	0.1346
0.6	0.1278
0.7	0.1297

As a result of Table 5.4 and 5.7, roll of factor of the interpolation filter may be selected as ρ=0.6 or ρ=0.7. Although interpolation filter with 0.5 roll of factor gives better results, it is not convenient for fading channel application.

Figure 5.22 shows the tracking performance of the proposed timing recovery scheme at 10 dB, 20 dB and 30 dB SNR, the rms error values are given in Table 5.8.

Table 5.8 The rms error values for the simulations in Figure 5.22.

Channel: *v*=90 km/h and f_c = 1800MHz, L_o =32, ρ =0.6, Method B	
SNR	**rms error**
10dB	0.1409
20dB	0.1301
30dB	0.1278

Table 5.5 and 5.8 gives the same conclusion; smaller SNR gives higher value of rms error.

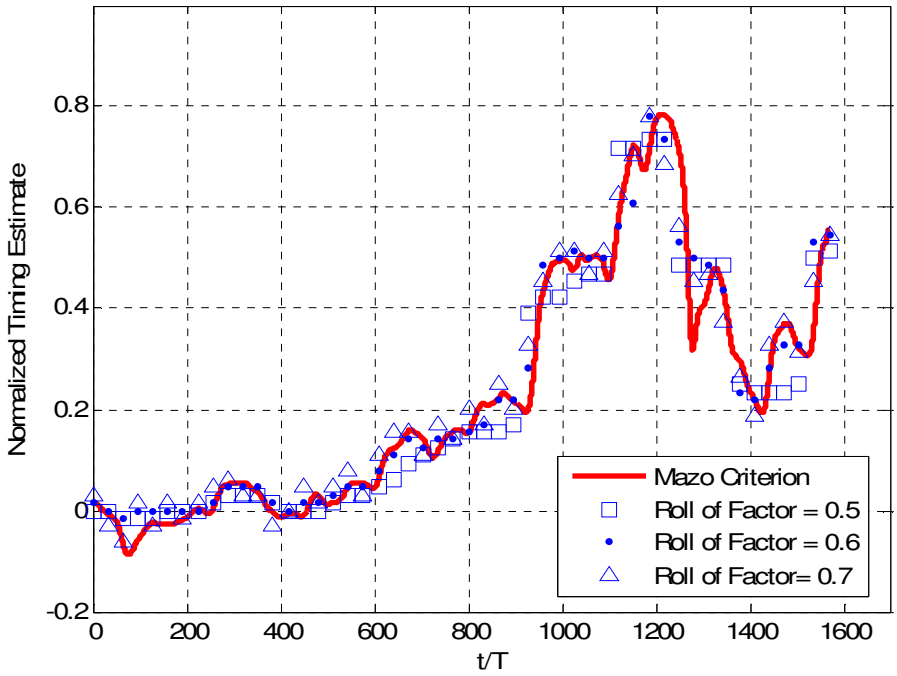

Figure 5.21 Tracking performance of the proposed synchronizer for different roll of factor values. (L_o =32, SNR=30dB, v=90 km/h and f_c= 1800MHz).

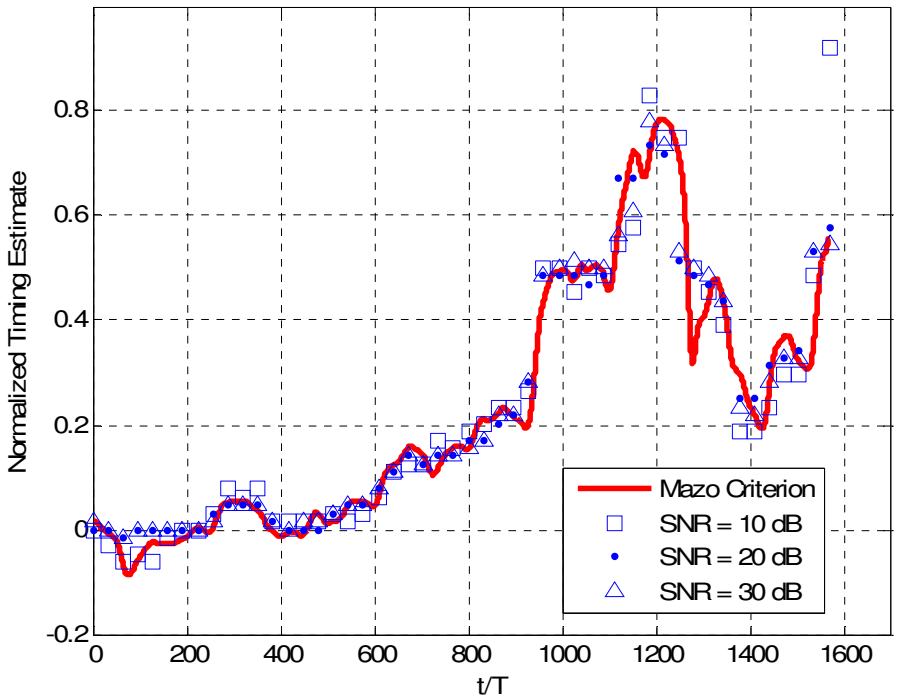

Figure 5.22 Tracking performance of the proposed synchronizer for different SNR values. (L_o =32, v=90 km/h and f_c= 1800MHz).

CHAPTER 6

CONCLUSION

Throughout this study, it has been noticed that although there are plenty of research studies on the area of symbol synchronization for CPM signals, there are still issues that are to be investigated in the frequency selective fading channel transmission area.

In this study, symbol timing recovery for CPM signals over multipath fading channel was examined by employing GMSK signal. The reason of choosing GMSK among the CPM family is its common use within digital communication systems like GSM and DECT.

In the GSM system, specific training sequences which have good crosscorrelation properties are used for channel identification. In this study, the channel identification solution based on correlation method was reviewed and the training sequences were presented. In order to take advantage of the good correlation property, the training sequences were used throughout the initial timing acquisition in simulations.

As it is mentioned in the literature, approximation of GMSK modulation as a linear modulation is necessary to enable the use of MLSE method in receiver. Consequently, the linearly approximated GMSK was reviewed, power spectrum density and waveform envelope of the linear GMSK signal were examined and

observed as expected. Time varying multipath fading channel with TU delay power profile has been simulated.

The performance of the recovery scheme in MSK over multipath fading channel was examined in [1] by using the proposed timing recovery scheme which was based on correlation (matched filter) method by using the samples of the received signal. The same matched filter could not be used for both MSK and GMSK modulation scheme due to different spanning duration of their pulse shapes. As a result, two methods; “Method A” and “Method B” were developed in order to construct the matched filter for the application on GMSK signals.

Tracking ability of the synchronizer by using both methods was simulated. In order to compare these methods rms error values were calculated by using Mazo criterion which is an important tool in the context. According to the simulation figures, it was observed that both methods could track channel variation successfully. However, it was assessed that Method B has a slightly better performance than Method A especially under fast fading channel conditions with respect to rms error values. Consequently, Method B was used for the simulations throughout the study.

Precise timing estimation was achieved by employing interpolation and iterative maximum search process. Moreover, interpolation filter structure was examined with simulations. The initial timing information was acquired by using a training sequence, placed in front of the data burst. Tracking mode is performed by tentative decisions from MLSE receiver in the proposed timing recovery [1]. However, in this study, tentative decisions were assumed to be error free and tracking mode was performed by them. Furthermore, Mazo criterion was used as a basis for the tracking performance of the proposed scheme.

Simulations were repeated for different value of parameters; length of observation interval, roll of factor of interpolation filter and SNR. By investigating

the effects of the parameters on the performance of the synchronizer, sensitivity analyses were performed.

As a future work, tentative decisions may be acquired from the MLSE receiver by using Viterbi Algorithm. The performance of the MLSE receiver depends on the available estimate of the channel impulse response. Therefore, channel estimation techniques (blind or non blind) may be investigated. Thus, the performance of the synchronizer may be tested in a more complex receiver model.

REFERENCES

[1] S. Sezginer, "Symbol Synchronization For MSK Signals Based On Matched Filtering," M.Sc. Thesis, Electrical and Electronics Eng. Dept., Middle East Technical University, Ankara, September 2003.

[2] S. Sezginer, Y. Tanık, "An Improved Matched Filter Based Symbol Synchronizer For MSK Transmission Over Fading Multipath Channels," IEEE Vehicular Technology Conference, vol. 3, pp. 1678 – 1682, Sept. 2004.

[3] J. G Proakis, "Digital Communications," Singapore, McGraw-Hill, 1995.

[4] S. Eken, "A Study on GMSK Modulation And Channel Simulation," M.Sc. Thesis, Electrical and Electronics Eng. Dept., Middle East Technical University, Ankara, Feb. 1994.

[5] M. C. Jeruchim, P. Balaban and K. S. Shanmugan, "Simulation of Communication Systems Modeling, Methodology, and Techniques," New York, Second Ed., Kluwer Academic, 2002.

[6] J. Eberspacher, H-J Vögel, C. Bettstetter, "GSM Switching, Services and Protocols," John-Wiley, Second Edition, 1999.

[7] P. A. Laurent, "Exact and Approximate Construction of Digital Phas Modulation by Superposition of Amplitude Modulated Pulses (AMP)," IEEE Trans. Commun., vol. Com-34, pp. 150-160, Feb. 1986.

[8] P. Jung, "Laurent's representation of binary digital continuous phase modulated signals with modulation index 1/2 revisited," IEEE Trans. Commun., vol. 42, pp. 221-224, 1994.

[9] A Wiesler, F. K. Jondral, “A software Radio For Second and Third Generation Mobile Systems ”, IEEE Trans. Commun., vol. Com-51, No 4, pp 738- 748 July 2002.

[10] A Wiesler, R. Machauer, F. Jondral, “Comparison of GMSK and Linear Approximated GMSK For Use In Software Radio”, IEEE, pp 557-560, 1998.

[11] B. Canpolat, “Design and Simulation of an Adaptive MLSE Receiver for GSM System,” M.Sc. Thesis, Electrical and Electronics Eng. Dept., Middle East Technical University, Ankara, Feb. 1994.

[12] A. Mehrotra, GSM System Engineering, Boston, Artech House, 1996.

[13] H. Meyr and G. Ascheid, Synchronization in Digital Communications, vol.1, New York: John Wiley & Sons, 1990.

[14] H. Meyr, M Moeneclaey, and S. A. Fechtel, Digital Communication, New York: McGraw-Hill, 1968.

[15] U. Mengali and A. N. D’Andrea, Synchronization Techniques for Digital Receivers, New York: Plenum Press, 1997.

[16] R. de Buda, ”Coherent Demodulation of Frequency Shift Keying with Low Deviation Ratio,” IEEE Trans. Commun., vol. COM-20, pp. 429-435, June 1972.

[17] T. Aulin and C. E. Sundberg, “Synchronization Properties of Continuous Phase Modulation,” in Proc. Int Conf. Commun., Philadelphia, PA, pp. D7.1.1-D7.1.7, June 1982.

[18] A. N. D’Andrea, U. Mengali, and R. Reggiannini, “Carrier Phase and Clock Recovery for Continuous Phase Modulated Signals,” IEEE Trans. Commun., vol. COM-35, pp. 1095-1101, Oct. 1987.

[19] J. Huber and W. Liu, “Data-Aided Synchronization of Coherent CPM Receivers,” IEEE Trans. Commun., vol. COM-40 pp. 178-189, Jan. 1992.

[20] R. Melhan, Y.E. Chen, and H. Meyr, “A Fully Digital Feedforward MSK Demodulator with Joint Frequency Offset and Symbol Timing Estimation for

Burst Mode Mobile Radio", IEEE Trans. Veh. Techol., vol. VT-42 pp. 434-443, Nov. 1993.

[21] U. Lambrette and H. Meyr, "Two Timing Recovery Algorithms for MSK," in Proc.ICC'94, New Orleans, LO, pp. 918-992, May 1994.

[22] M. Morelli and G. M. Vitetta, "Two Timing Recovery Algorithms for MSK," in Proc. ICC'94, New Orleans, LO, pp. 1997-1999, Dec. 2000.

[23] F. Patenaude, J. H. Lodge, and P. A. Galko, "Symbol Timing Tracking for Continuous Phase Modulation over Fast Flat-Fading Channels," IEEE Trans. Veh. Technol., vol. VT-40 pp. 615-626, Aug. 1991.

[24] L.E. Franks, "Carrier and Bit Synchronization in Data Communication- A Tutorial Review," IEEE Trans. Commun., vol. COM-28, pp. 1107-1120, Aug. 1980.

[25] L. P. Sabel, "Maximum Likelihood Approach to Symbol Timing Recovery in Digital Communications," Ph.D. Thesis, Sch. Of Elec. Eng. Univ. South Australia, South Australia, Oct. 1993.

[26] H.L. Van Trees, Detection, Estimation and Modulation Theory Part I, New York: John Wiley & Sons, 1968.

[27] K. H. Muller and M. Muller, "Timing Recovery in Digital synchronous Data Receivers," IEEE Trans. Commun., vol. COM-24, pp. 516-531, May 1976.

[28] J. E. Mazo, "Optimum Timing Phase for an Infinite Equalizer," Bell Syst, Tech. J., vol. 54, pp. 189-201, 1975.

[29] R. W. Lucky, J. Salz, and E. J. Weldon, Jr., Principals of Data Communication, New York: McGraw-Hill, 1968.

[30] A. V. Oppenheim and R. W: Schafer, Discrete-Time Signal Processing, Upper Saddle River, NJ: Prentice-Hall, 1999.

[31] A. N. D'Andrea, U. Mengali, and M. Morelli, "Symbol Timing Estimation with CPM Modulation," IEEE Trans. Commun., vol. COM-44, pp. 1362-1372, Oct. 1996.

[32] R. Steele, Chin-Chun Lee, P. Gould, GSM, cdmaOne and 3G Systems, West Sussex, John Wiley & Sons ltd., 2001.

APPENDIX A

CPM SIGNALS

Continuous phase modulation (CPM) conserves and reduces signal energy and bandwidth at the same time. CPM is a constant envelope, nonlinear modulation method with memory. The constant envelope property of CPM schemes makes possible to use non-linear amplifiers. The phase is a continuous function of time since the data symbols modulate the instantaneous phase of the transmitted signal.

A.1 SIGNAL MODEL

The complex envelope of a CPM signal is given by [31]

$$s(t) = \sqrt{\frac{2E_s}{T}} e^{i(\theta + \phi(\alpha; t-\tau))}, \qquad \text{(A.1)}$$

where E_s is the energy per signaling interval, T is the symbol period, θ is carrier phase, τ is timing epoch, $\boldsymbol{\alpha} = \{ \alpha_i \}$ are data sequence from the alphabet $\{\pm 1, \pm 3, \ldots, \pm(M-1)\}$ and $\phi(\boldsymbol{\alpha}, t)$ is the information-bearing phase:

$$\phi(\alpha;t) = 2\pi \sum_i h_i \alpha_i q(t - i\tau) . \quad \text{(A.2)}$$

The parameter h_i is called the modulation index.. When h_i =h for all i, the modulation index is fixed for all symbols. When the modulation index varies from one symbol to another, the CPM signal is called multi-h. q(t) is the phase pulse of the modulator, which is related to the frequency pulse g(t) by

$$q(t) = \int_{-\infty}^{t} g(\tau) d\tau , \quad \text{(A.3)}$$

and is normalized in such a way that

$$q(t) = \begin{cases} 1/2, & t \geq LT \\ 0 \quad , & t<0 \end{cases} . \quad \text{(A.4)}$$

The phase pulse is nonzero in the interval t ∈ (0, LT), where L is an integer called the correlation length. If L=1, the modulated signal is called full response CPM. If L>1, the modulated signal is called *partial response CPM.* The CPM signal has memory that is introduced through the phase continuity. For L>1, additional memory is introduced in the CPM signal by the pulse g(t).

By choosing different frequency pulses and varying the parameters h and M, a great variety of CPM schemes may be formed.

A.2 MINIMUM SHIFT KEYING AND GAUSSIAN MINIMUM SHIFT KEYING

A subset of CPM signals is minimum shift keying (MSK) corresponds to h=1/2, M=2 and a rectangular frequency pulse

$$g(t)=\begin{cases}1/2T, & 0< t \le T \\ 0 \quad , & \text{elsewhere}\end{cases}. \tag{A.5}$$

MSK modulation is a constant envelope digital modulation. The spectrum of MSK is quite large and substantial energy exists in the sidelobes.

The spectrum of an MSK modulated signal may be compressed by filtering the modulating baseband pulses to produce much smoother changes in frequency, thereby compressing the bandwidth of the modulated signal. The type of filter used has a Gaussian impulse response and the resulting modulation scheme is called Gaussian MSK (GMSK). The relative bandwidth of the Gaussian filter defines the spectrum compression that is achieved, i.e. a smaller filter bandwidth results in a narrower modulated spectrum. Unfortunately, the Gaussian filter also introduces ISI whereby each modulation symbol spreads into adjacent symbols [32].

In this thesis, the emphasis is given on Gaussian MSK (GMSK), which is used as the GSM modulation scheme. GMSK is obtained by letting h=1/2, M=2 and g(t) is given by,

$$g(t)=h(t)* rect(t/T). \tag{A.6}$$

Gaussian shaped impulse response*, h(t)* is given by;

$$h(t)=\frac{1}{\sqrt{2\pi}\sigma T}\exp\left(-\frac{t^2}{2\sigma^2T^2}\right), \tag{A.7}$$

where

$$\sigma=\sqrt{\ln 2}/2\pi BT \tag{A.8}$$

here, B is the 3 dB bandwidth of the filter.

rect (t/T) is defined by;

$$rect(t/T)=\begin{cases}1/T, & |t|<T/2\\ 0\ , & \text{otherwise}\end{cases}, \tag{A.9}$$

then,

$$g(t)=\frac{1}{2T}\left[erf\left(-\frac{\sqrt{2}\pi B(t-T/2)}{\sqrt{\ln 2}}\right)+erf\left(-\frac{\sqrt{2}\pi B(t+T/2)}{\sqrt{\ln 2}}\right)\right], \tag{A.10}$$

where

$$erf(x)=\frac{2}{\sqrt{\pi}}\int_0^x \exp(-\upsilon^2)d\upsilon \tag{A.11}$$

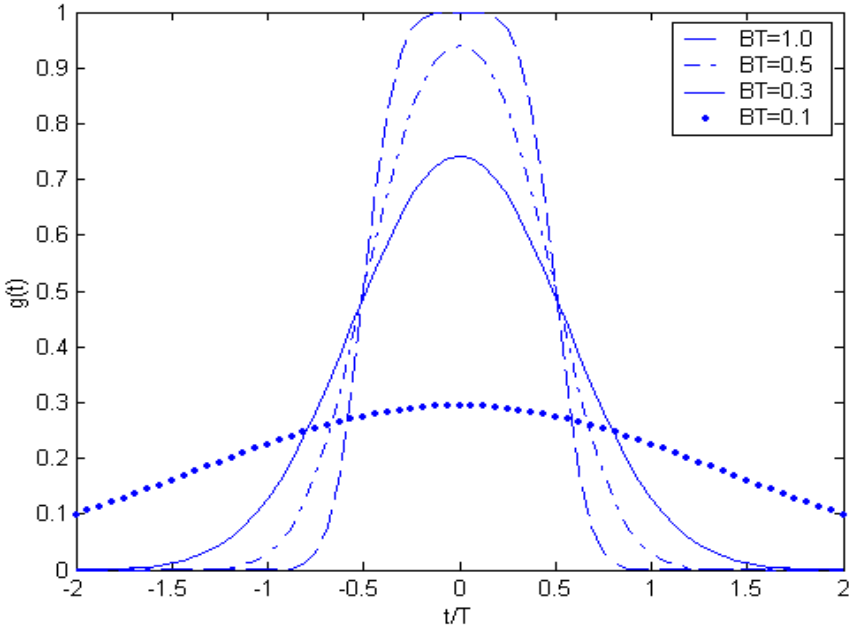

Figure A.1 Impulse Response of *g(t)*

The resulting impulse response *g(t)* is given in Fig A.1 for some values of BT. Notice that with decreasing BT the impulse response becomes broader. For BT $\rightarrow \infty$ it converges to rect(.) function, also GMSK signal converges to MSK signal. The Gaussian low-pass filtering has the effect of additional smoothing but also of the broadening the impulse response *g(t).* This means that, the power spectrum of the signal is made narrower, but on the other hand the individual impulse responses are "smeared" across several bit durations, which leads to increase intersymbol interference.

APPENDIX B

APPROXIMATION OF GMSK TO LINEAR QAM SIGNAL

The GMSK signal can be approximated to a linear QAM signal by adopting a suitable pulse shape [4]. The pulse shape happens to be an approximately Gaussian function spanning a time interval of approximately four symbol durations as will be derived in this appendix.

The phase expression of GMSK signal is given as;

$$\phi(t) = \int_{-\infty}^{t} \frac{\pi}{2} \sum_{k} a_k \, g(\tau - kT) d\tau, \tag{B.1}$$

which can also be expressed as;

$$\phi(t) = \frac{\pi}{2} \sum_{k} a_k \int_{-\infty}^{t-kT} g(\tau) d\tau, \tag{B.2}$$

where a_k's are the differentially encoded bits in the form of ± 1, and g(t) is the shaping function given as;

$$g(t) = \frac{1}{2T}\left[erf\left(-\frac{\sqrt{2}\pi B(t - T/2)}{\sqrt{\ln 2}}\right) + erf\left(\frac{\sqrt{2}\pi B(t + T/2)}{\sqrt{\ln 2}}\right)\right]. \quad \text{(B.3)}$$

To simplify equation (B.2), a new function β(t) can be defined as;

$$\beta(t) = \frac{\pi}{2}\int_{-\infty}^{t} g(\tau)d\tau. \quad \text{(B.4)}$$

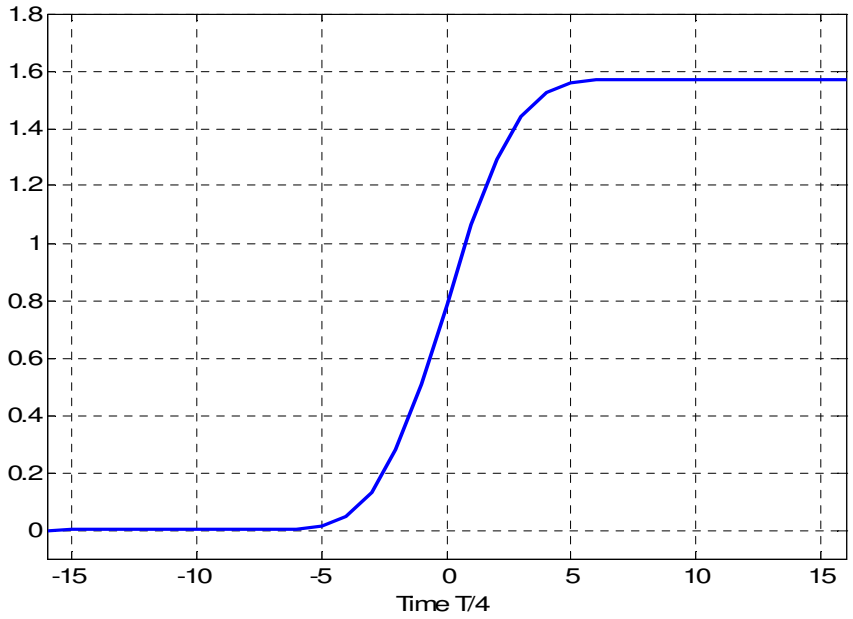

Figure B.1 Shape of β(t)

As seen in Figure B.1, β(t) is equal to π/2 when t ≥ 3T/2, since the area under g(t) is equal to 1 when t ≥ 3T/2.

Then, the phase can be expressed as;

$$\phi(t) = \sum_{k} a_k \beta(t - kT). \quad \text{(B.5)}$$

Thus, the baseband GMSK signal can be rewritten as;

$$s_b(t)=\exp j\left[\sum_k a_k \beta(t-kT)\right], \tag{B.6}$$

Now consider the time interval $(2n-1)T/2 \le t \le (2n+1)T/2$. For this interval, if $k \le (n-2)$ then $\beta(t-kT)= \pi/2$ since in this case $(t-kT) \ge 3T/2$. Therefore, the above equation can be rewritten as;

$$s_b(t)=\exp j\left[\sum_{k=-\infty}^{n-2} a_k \beta(t-kT)+\sum_{k=n-1}^{n+1} a_k \beta(t-kT)\right], \tag{B.7}$$

and for the time interval $(2n-1)T/2 \le t \le (2n+1)T/2$ one can get;

$$s_b(t)=\exp j\left[\frac{\pi}{2}\sum_{k=0}^{n-2} a_k\right]\exp j\left[\sum_{k=n-1}^{n+1} a_k \beta(t-kT)\right], \tag{B.8}$$

$$s_b(t)=\exp j\left[\frac{\pi}{2}\sum_{k=0}^{n-2} a_k\right]\prod_{k=-1}^{1}\exp j\left[a_{n-k}\beta(t-(n-k)T)\right], \tag{B.9}$$

In the light of above equations, it can be shown that [4] the baseband GMSK signal may be expressed as;

$$s_b(t)=\sum_{N=-\infty}^{\infty}\sum_{k=0}^{3}\exp j\frac{\pi}{2}\left[\sum_{n=-\infty}^{N} a_n-\sum_{i=1}^{2} a_{N-i}\alpha_{ki}\right]C_k(t-NT), \tag{B.10}$$

where,

$$\alpha_{01}=0 \qquad \alpha_{11}=1 \qquad \alpha_{21}=0 \qquad \alpha_{31}=1$$

$\alpha_{02} = 0 \qquad \alpha_{12} = 0 \qquad \alpha_{22} = 1 \qquad \alpha_{32} = 1$

and the functions $C_k(t)$, k=0,1,2,3 are defined by;

$$
\begin{aligned}
C_0(t) &= \sin[\beta(t-T)]\sin[\beta(t)]\sin[\beta(t+T)] && \frac{-T}{2} \le t \le \frac{T}{2} \\
&= \sin[\beta(t-T)]\sin[\beta(t)]\sin\left[\frac{\pi}{2} - \beta(t-2T)\right] && \frac{T}{2} \le t \le \frac{3T}{2} \\
&= \sin[\beta(t-T)]\sin\left[\frac{\pi}{2} - \beta(t-3T)\right]\sin\left[\frac{\pi}{2} - \beta(t-2T)\right] && \frac{3T}{2} \le t \le \frac{5T}{2} \\
&= \sin\left[\frac{\pi}{2} - \beta(t-4T)\right]\sin\left[\frac{\pi}{2} - \beta(t-3T)\right]\sin\left[\frac{\pi}{2} - \beta(t-2T)\right] && \frac{5T}{2} \le t \le \frac{7T}{2} \\
&= 0 && \text{elsewhere}
\end{aligned}
\tag{B.11}
$$

$$
\begin{aligned}
C_1(t) &= \sin[\beta(t-T)]\sin[\beta(t+T)]\sin\left[\frac{\pi}{2} - \beta(t)\right] && \frac{-T}{2} \le t \le \frac{T}{2} \\
&= \sin[\beta(t-T)]\sin\left[\frac{\pi}{2} - \beta(t-2T)\right]\sin\left[\frac{\pi}{2} - \beta(t)\right] && \frac{T}{2} \le t \le \frac{3T}{2} \\
&= 0 && \text{elsewhere}
\end{aligned}
\tag{B.12}
$$

$$
\begin{aligned}
C_2(t) &= \sin[\beta(t-T)]\sin[\beta(t)]\sin\left[\frac{\pi}{2} - \beta(t+T)\right] && \frac{-T}{2} \le t \le \frac{T}{2} \\
&= 0 && \text{elsewhere}
\end{aligned}
\tag{B.13}
$$

$$
\begin{aligned}
C_3(t) &= \sin[\beta(t-T)]\sin\left[\frac{\pi}{2} - \beta(t)\right]\sin\left[\frac{\pi}{2} - \beta(t+T)\right] && \frac{-T}{2} \le t \le \frac{T}{2} \\
&= 0 && \text{elsewhere}
\end{aligned}
\tag{B.14}
$$

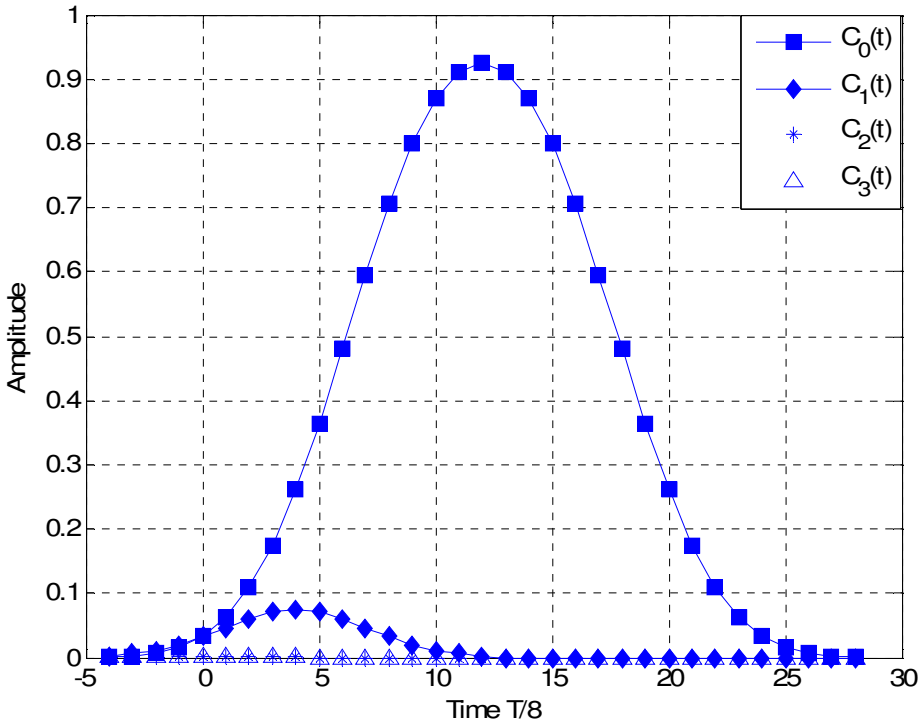

Figure B.2 Comparison of $C_0(t)$, $C_1(t)$, $C_2(t)$ and $C_3(t)$

In Figure B.2, the four functions $C_0(t)$, $C_1(t)$, $C_2(t)$ and $C_3(t)$ are sketched. It is observed that the functions other than $C_0(t)$ may be neglected since the contribution of these functions to the summation in equation (B.10) is not considerable as compared to that of $C_0(t)$.

Thus, with this simplification, the baseband modulated GMSK signal can be approximated as;

$$s_b(t) \cong \sum_n \exp j\left[\frac{\pi}{2}\sum_{i=-\infty}^{n} a_i\right] C_0(t-nT)\,. \qquad \text{(B.15)}$$